SOLAR SAIL ATTITUDE DYNAMICS AND CONING CONTROL: On Developing Control Methods for Solar Sail Coning at Orbit Rate to Attain Desired Orbital Effects

Farheen Rizvi

M.S./B.S. Concurrent Degree Candidate, 2010

A thesis submitted to the

Faculty of the Graduate School of the

University of Colorado in partial fulfillment

of the requirements for the degree of

Master of Science

Department of Aerospace Engineering Sciences

2010

This thesis entitled:

Solar Sail Attitude Dynamics and Coning Control: On Developing Control Methods for Solar

Sail Coning at Orbit Rate to Attain Desired Orbital Effects

written by Farheen Rizvi

has been approved for the Department of Aerospace Engineering Sciences

_____

Dr. Dale A. Lawrence

_____

Dr. Hanspeter Schaub

Date:_____

The final copy of this thesis has been examined by the signatories, and we
find that both the content and the form meet acceptable presentation standards
of scholarly work in the above mentioned discipline

Rizvi, Farheen (M.S. Aerospace Engineering Sciences)
Solar Sail Attitude Dynamics and Coning Control: On Developing Control Methods for Solar Sail Coning at Orbit Rate to Attain Desired Orbital Effects
Thesis Directed by Professor Dale A. Lawrence

In this thesis, a control method is developed for the solar sail normal vector to trace a desired circular coning trajectory at orbit rate. The coning trajectory is defined in the local vertical local horizontal (LVLH) frame and the coning occurs about an LVLH equilibrium sail attitude. Past research has shown that sail attitude equilibria exist in the LVLH frame under the influence of aerodynamic, gravity gradient and solar torques. Precession of the sail normal from these equilibria causes sail normal coning about that equilibrium attitude. If the coning happens at orbit rate, wide variety of orbital effects can be induced with minimum excitation of the sailcraft structure. This results in an inexpensive spacecraft with a longer duration mission as compared to other conventional efforts. A special case of analyzing circular cones (at orbit rate coning) revealed that new Sun-synchronous orbits were created and launch injection errors were overcome by employing the sail coning method. The control method herein minimizes the angular momentum error between the sail and desired angular momentum vectors at orbit rate. Since angular momentum is a function of sail normal, angular momentum error reduction raises hope in reducing the sail normal error between the sail normal and desired sail normal vector as well. The results show that even though the control method enables the sail angular momentum to track the desired angular momentum on the coning trajectory, the sail normal tracing can only occur about certain LVLH equilibrium points, for small cones and small initial condition angular position/velocity errors. The control method is robust for tracking the desired angular momentum at orbit rate, but not always for tracking the desired sail normal. The case where the sail normal does track the desired at orbit rate corresponds to tracing a 1° circular cone about an orbit

lowering LVLH equilibrium point. Even though the control torques are on the order of 10^{-6} Nm (acceptable on small sailcraft) for both a spinning and non-spinning sail, a spinning sail (spun at a specific rate) requires less control torque (4 times lower than a non-spinning sail) to yield the desired orbit rate circular coning. The control torques can be applied to the sailcraft to enable orbit rate cone tracing of the sail normal and yield the desired orbital effects.

This thesis is dedicated to all the people who will benefit from my work.

ACKNOWLEDGEMENTS

I am deeply indebted to Prof. Dale Lawrence for being an excellent and kind mentor throughout this research work. I greatly appreciate his guidance, support, enthusiasm and clear perspective, which enabled me to finish this work with much interest. His patience and humility has moved me as a student and as an individual. In addition, his presence throughout this work was very encouraging.

I would also like to extend my sincere thanks to Jay McMahon (PhD candidate, Aerospace Engineering Sciences, CU-Boulder) for helping me with the literature search and for answering questions about my thesis. I am grateful to Prof. Eric Frew and Prof. Hanspeter Schaub for serving on my thesis committee.

Lastly, I express my sincere gratitude to Rizwan Qureshi (NASA Goddard Space Flight Center) for providing me with invaluable support and much comfort during challenging times throughout my thesis work.

CONTENTS

LIST OF TABLES

LIST OF FIGURES

NOMENCLATURE

$A - frame$ →   inertial frame

$\hat{x}, \hat{y}, \hat{z}$ →   unit vectors forming right-handed coordinate system for the A-frame
($\hat{x}$ points along the vernal equinox, $\hat{z}$ normal to the Equatorial plane, $\hat{y}$ lies in the Equatorial plane)

$B - frame$ →   a principal frame (due to axi-symmetric mass properties), describes sail tip and tilt velocities relative to the L-frame

$\hat{n}, \hat{l}, \hat{m}$ →   unit vectors forming right-handed coordinate system for the B-frame, frame moves with sail normal tip and tilt but not with rotation about its normal ($\hat{n}$ points along the sail normal, $\hat{l}$ and $\hat{m}$ lie in the plane of the sail)

$C - frame$ →   sail body-fixed frame

$\hat{n}, \hat{p}, \hat{q}$ →   unit vectors forming right-handed coordinate system for the C-frame
($\hat{n}$ points along the sail normal, $\hat{p}$ and $\hat{q}$ lie in the plane of the sail)

$L - frame$ →   local vertical local horizontal frame

$\hat{r}, \hat{v}, \hat{o}$ →   unit vectors forming right-handed coordinate system for the L-frame
($\hat{r}$ points along the orbit radius, $\hat{v}$ is in the sail velocity direction, $\hat{o}$ is along the sail angular momentum vector)

L →   square sail side length [m]

A →   sail area [m^2]

r_c →   distance to the sailcraft bus from the sail plane in the sail normal direction [m]

m_s →   sail mass [kg]

m_b →   sailcraft bus mass [kg]

s →   sail reflectivity

I_s →   inertia tensor [kgm^2]

I_n →   axial moment of inertia [kgm^2]

I_T	$\rightarrow$	transverse moment of inertia [kgm^2]
a	$\rightarrow$	orbit altitude [km]
i	$\rightarrow$	orbit inclination [deg]
Ω	$\rightarrow$	orbit right ascension of ascending node [deg]
r_s	$\rightarrow$	right ascension of Sun [deg]
d_s	$\rightarrow$	declination of Sun [deg]
F_s	$\rightarrow$	solar flux at 1 AU [W/m^2]
$\hat{n}$	$\rightarrow$	sail normal unit vector
$\hat{n}_c$	$\rightarrow$	desired sail normal unit vector (on the desired cone)
$\hat{n}_0$	$\rightarrow$	sail equilibrium attitude in the L-frame
$\Delta\hat{n}$	$\rightarrow$	sail normal error between $\hat{n}$ and $\hat{n}_c$
β	$\rightarrow$	cone angle (angle between and sail normal vector in deg)
ϕ	$\rightarrow$	clock angle (angle between $\hat{v}$ and projection of sail normal onto the $\hat{r} - \hat{v}$ plane in deg)
β_0	$\rightarrow$	equilibrium cone angle [deg]
ϕ_0	$\rightarrow$	equilibrium clock angle [deg]
β_c	$\rightarrow$	desired cone angle [deg]
ϕ_c	$\rightarrow$	desired clock angle [deg]
$\delta\beta$	$\rightarrow$	angular measure for cone perturbation from the equilibrium point [deg]
δ	$\rightarrow$	half cone angle and euler (rotation) angle for the rotation matrix [deg]
R_c^0	$\rightarrow$	rotation matrix for calculating $\hat{n}_c$ by rotating $\hat{n}_0$ through an euler axis and angle

$\hat{E}$ $\rightarrow$ euler (rotation) axis

${}^{A}\vec{\omega}_{C}$ $\rightarrow$ angular velocity of the C-frame as seen in the A-frame [rad/s]

$\omega_{1}, \omega_{2}, \omega_{3}$ $\rightarrow$ B-frame components of ${}^{A}\vec{\omega}_{C}$ angular velocity from the simulation [rad/s]

${}^{A}\vec{\omega}_{B}$ $\rightarrow$ angular velocity of the B-frame as seen in the A-frame [rad/s]

${}^{L}\vec{\omega}_{B}$ $\rightarrow$ angular velocity of the B-frame as seen in the L-frame (describes sail tip and tilt velocities with respect to the L-frame in rad/s)

${}^{L}\vec{\omega}_{B}^{*}$ $\rightarrow$ desired angular velocity [rad/s]

$\omega_{\perp}$ $\rightarrow$ dot product of orbit rate velocity and sail normal vector [rad/s]

$\vec{\omega}_{T}$ $\rightarrow$ projection of ${}^{A}\vec{\omega}_{B}$ onto the plane orthogonal to the sail normal vector [rad/s]

ω_{n} $\rightarrow$ inertial sail spin rate [rad/s]

ω_{no} $\rightarrow$ equilibrium sail inertial spin rate [rad/s]

ω_{nc} $\rightarrow$ desired inertial sail spin rate [rad/s]

ω_{s} $\rightarrow$ sail spin rate about the sail normal vector relative to the B-frame [rad/s]

ω_{o} $\rightarrow$ orbit rate [rad/s]

${}^{A}\vec{h}_{C}$ $\rightarrow$ inertial sailcraft angular momentum of the C-frame as seen in the A-frame [kgm^{2}/s]

$\vec{h}$ $\rightarrow$ angular momentum vector [kgm^{2}/s]

$\vec{h}_{c}$ $\rightarrow$ desired angular momentum vector [kgm^{2}/s]

$\vec{h}_{S}$ $\rightarrow$ angular momentum vector from the sail simulation [kgm^{2}/s]

$\Delta {}^{A}\vec{h}_{C} / \Delta \vec{h}$ $\rightarrow$ angular momentum error [kgm^{2}/s]

Δn_term $\rightarrow$ contribution from sail orientation terms in the angular momentum error [kgm^2/s]

$\Delta \omega\_term$ $\rightarrow$ contribution from angular velocity terms in the angular momentum error [kgm^2/s]

$\vec{\tau}$ $\rightarrow$ net external torque acting on the sail [Nm]

$\vec{\tau}_n$ $\rightarrow$ normal component of the net torque acting on the sail [Nm]

$\vec{\tau}_T$ $\rightarrow$ transverse component of the net torque acting on the sail [Nm]

$\vec{\tau}_a$ $\rightarrow$ aerodynamic torque [Nm]

τ_{am} $\rightarrow$ aerodynamic moment coefficient [Nm]

$\vec{\tau}_s$ $\rightarrow$ solar torque [Nm]

τ_{sm} $\rightarrow$ solar moment coefficient [Nm]

$\vec{\tau}_g$ $\rightarrow$ gravity gradient torque [Nm]

τ_{gm} $\rightarrow$ gravity moment coefficient [Nm]

$\tau_{control}$ $\rightarrow$ control torque [Nm]

τ_S $\rightarrow$ total torque from the simulation [Nm]

τ_c $\rightarrow$ total torque required to be on the desired coning trajectory [Nm]

τ_{Se} $\rightarrow$ environmental torque from the simulation [Nm]

τ_{ce} $\rightarrow$ environmental torque of the desired coning trajectory [Nm]

τ_{stay_cone} $\rightarrow$ additional torque required to stay on the desired cone [Nm]

V $\rightarrow$ Lyapunov function [(kgm^2/s)^2]

$k_{control}$ $\rightarrow$ control gain [1/s]

θ_e $\rightarrow$ angular position error [deg]

d $\rightarrow$ angular deviation which is added to the system to yield initial condition error [deg]

$\hat{N}_E$ $\rightarrow$ L-frame equilibrium attitude

θ $\rightarrow$ angular deviation from the L-frame equilibrium attitude [deg]

C_T $\rightarrow$ coning trajectory

$cp - cm$ $\rightarrow$ center of pressure to center of mass offset

r_{cp-cm} $\rightarrow$ cp-cm offset [m]

ρ $\rightarrow$ atmospheric density [kg/m^3]

C_D $\rightarrow$ coefficient of drag

$\hat{s}$ $\rightarrow$ sailcraft Sun vector

P $\rightarrow$ solar pressure [N/m^2]

f_s $\rightarrow$ specular reflectance fraction

t $\rightarrow$ time [s]

I. INTRODUCTION

I.1. Advantages of Solar Sail Technology

Solar sails are an attractive solution for expensive and massive space missions. Traditional spacecraft must carry in-space propulsion fuel that increases both launch mass and cost. A sail exposed to solar radiation offers free and continuous propulsion by manipulating the sail thrust vector direction relative to the Sun. Figure 1 illustrates a simple solar sail configuration and Figure 2 shows how the solar radiation thrust force is used for propulsion.
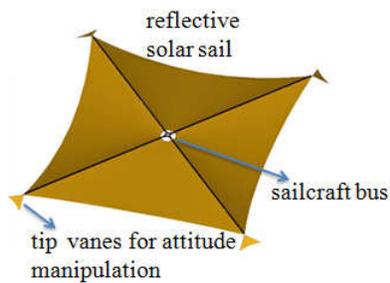
Figure 1: Solar sail configuration
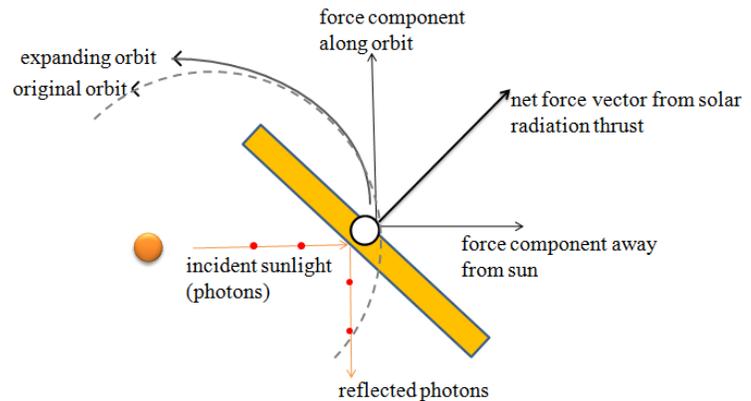
Figure 2: Solar radiation thrust force

A solar sail consists of a sailcraft bus that houses the necessary electronics and hardware, a large, reflective, gossamer sail and an attitude manipulation component (tip vanes, thrusters, reaction wheels). The integrated effect of the reflected photons provides the propulsive thrust force. A large sail area is required in order to interrupt the photon radiation and produce an appreciable amount of thrust force. Since acceleration is inversely proportional to mass for a given thrust force, the mass of the sailcraft must be kept to a minimum. Thus, the sail and bus are designed to provide a large area-to-mass ratio and maximize the propulsion acceleration. Incident rays of sunlight reflect off of the sail (assume specular reflection from a perfectly flat sail) and produce

two force components: one in the direction of the incident sunlight and another in the opposite direction of the reflected rays. In the net force vector, the components tangent to the sail surface cancel and the components normal to the surface add to produce the thrust force approximately in the sail normal direction. NASA's CubeSail project used a perfectly reflective 40 m^2 square sail in simulation to show that at 1 AU from the Sun, 0.03 N of solar radiation thrust force can be produced [27]. Although this force is relatively small compared with other propulsion methods, it is available continuously and hence can still be used to propel spacecraft for long distances without carrying any propellant.

The free propulsion from solar radiation makes extended mission durations feasible with reduced spacecraft mass and cost. A typical science mission is expected to cost on the order of one million dollars per kilogram of spacecraft mass [27]. This leaves high potential for low-cost science missions that have reduced spacecraft mass. As an example, results from a comet rendezvous mission study to reach Comet 88P/Howell using chemical propulsion and solar sailing are shown in Figure 3.

[Rizvi, et. al. 2009]   [Stough, et. al. 2008]
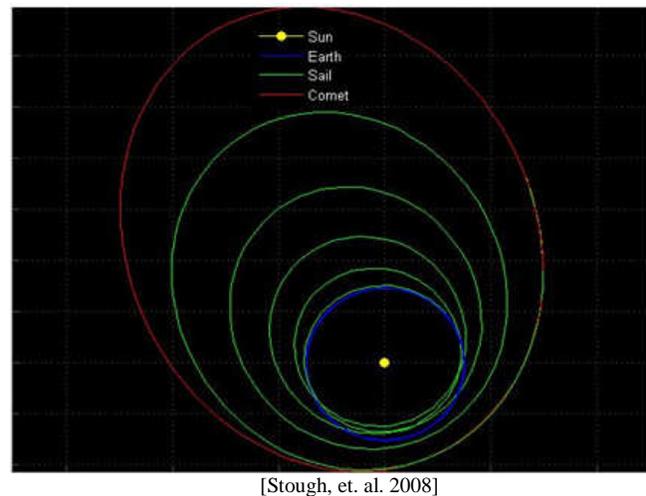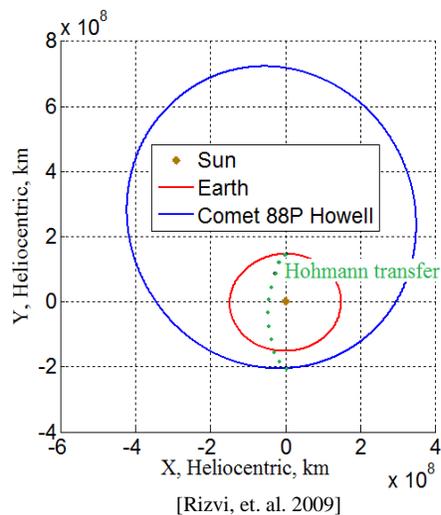
Figure 3: Comet Rendezvous Mission Study Using Chemical and Solar Sail Propulsion

Via traditional chemical propulsion, a Hohmann transfer from the Earth to the comet required 400 kg of propellant mass, whereas the solar sail completed the same mission with a total

spacecraft mass of 3 kg (a factor of ~135 reduction in spacecraft mass). This translates into lower launch costs to Earth escape velocity and reduced development costs for the spacecraft [21]. The transfer time for the high thrust approach using chemical propulsion was 0.7 years as compared with 10 years for the solar sail. Therefore, for missions where transfer time is not a critical parameter, solar sail propulsion can result in significant fuel mass savings.

The significant solar thrust propulsion enables non-Keplerian orbits for solar sails. With this unique capability of solar sails, many space science missions can be achieved which are difficult to implement using conventional (chemical) propulsion techniques. Conventional propulsion can only produce Keplerian orbits such as ellipses, parabola and hyperbola (parts of a conic section). However, non-Keplerian orbits can be produced with constant sail thrusting through which orbit raising and precession can be achieved. One such mission is the study of the Earth magnetotail for which non-Keplerian orbits are desired. This requires the spacecraft orbit to continuously rotate to follow a Sun-synchronous path and also raise its orbit to explore the entire magnetotail. Two mission scenarios using conventional and solar sail propulsion are illustrated in Figure 4.
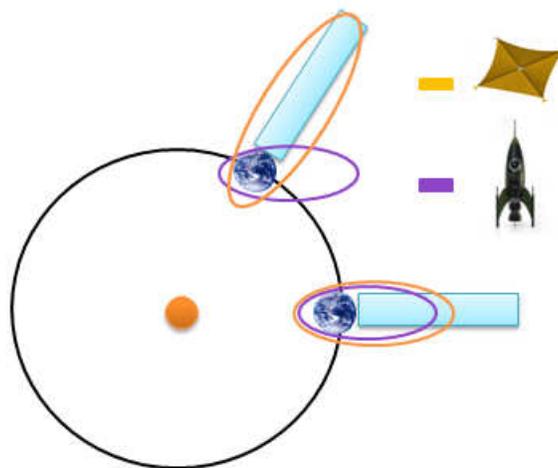
Figure 4: Exploring Earth Magnetotail Using Chemical and Solar Sail Propulsion

The chemical propulsion (purple line – rocket) with fuel enough for initial orbit injection produces an elliptical orbit, which then stays inertially fixed as the Earth (along with the magnetotail) rotates about the Sun. Since the magnetotail rotates with the Sun-Earth line, an inertially fixed Keplerian orbit with spacecraft apogee inside the magnetotail provides less than three months of science data. The spacecraft collects data for a limited time until the magnetotail rotates away with the Earth. In contrast, the solar sail propulsion system provides a unique steering capability that enables long-term residence within the magnetotail. In addition, the sail orbit can also be raised to provide full coverage of the magnetotail. The solar sail propulsion (yellow line – sail) allows the semi-major axis of the orbit to increase and precess with the Earth rotation. With a continuous Sun-synchronous apse-line precession to rotate and raise an elliptical Earth orbit, at least two years of scientific data could be returned [11]. Solar sail propulsion may provide an optimum propulsion system over conventional chemical propulsion, at least in some missions. It may also have advantages over electric propulsion due to the ease in attaining non-Keplerian orbits with reduced mission mass and cost [5].

I.2. *Solar Sail Previous Research and Challenges*

Solar sail research has conducted orbit, attitude and structural analysis. The orbit analysis focuses on producing orbit raising/lowering and inducing orbital effects using the sails. These effects can yield otherwise expensive orbits such as Sun-synchronous and halo types. In order to achieve the desired orbital effects, the sail must operate at the required attitude to modulate the solar thrust. Thus, orbit analysis has also motivated the research work on sail attitude manipulation. This is the focus of the thesis. Most of the orbit and attitude research have made simplifying assumptions on the sail structural conditions, and these assumptions are made here as well. Detailed structural analysis becomes important once the orbit and attitude analysis proves

feasibility based on the simplified model. A realistic structural analysis is then be needed to answer questions related to sail shape deformations, sail behavior once deployed in space and modeling imperfect sails due to variations in mass distribution and reflective sail surface quality.

The coning control approach in this thesis is particularly appropriate for gossamer sail structural dynamics because it uses minimum control torque and smooth sail motion due to the sail operation around a fixed equilibrium attitude with circular coning at orbit rate. Since the orbit rate is low compared to sail structural mode frequencies, excitation of structural modes is unlikely.

Details of previous work in the above topics are provided below.

I.2.1.   *Orbit Analysis*

The free and continuous propulsion from the sun provides an inexpensive solution for altering the orbital parameters of the sailcraft. Semi-major axis changes in the orbit can provide orbit raising or lowering. Sail orbit raising can be used to escape from the planetary gravitation field. Sands analyzed an escape maneuver from the Earth gravitational field using the solar thrust force [25]. Using a flat, perfectly reflective sail that rotated about its axis at half the orbit rate, solar sailing was found to accelerate a payload to escape condition in several months from near-Earth orbit. Apart from orbit raising and lowering, many other orbital effects can also be induced from the solar propulsion. Oyama, et. al. have investigated the orbital dynamics of an Earth-orbiting solar sail in which argument of perigee and eccentricity variations emerged [18]. A simple steering law in which the sail was directed along the Sun line at all times in the orbit could generate the necessary orbital effects. This line of apse precession, coupled with eccentricity variations was used to examine the Earth magnetotail. The argument of perigee

changes allowed the sail to rotate along with the Earth-Sun line, while the eccentricity changes enabled the sail to provide full area coverage of the magnetotail (in length and width).

Apart from providing orbital effects, a solar sail can be operated at halo orbits about the created artificial Lagrange points. One application of this is to provide early warnings of solar plasma storms [20]. Geomagnetic storms can cause significant difficulties near the Earth, such as loss of spacecraft or degradation of GPS signals, and can even be lethal for astronauts performing extravehicular activity. Such events can be accurately predicted by monitoring the upcoming solar wind and can be detected by spacecraft instruments (particle detectors and magnetometers) located between the Sun and the Earth. One possible location is to place the spacecraft at the L1 Lagrangian point of the Sun-Earth system. Lying 1.5 million kilometers upstream from the Earth, it provides an opportunity to detect storms one hour before the corresponding solar wind reaches the Earth. In case the spacecraft was located further upstream from the Earth, the storm detection could be made earlier. Prado, et. al. have proposed that a Sun-facing solar sail can be used to place a sailcraft 3 million kilometers away from the Earth such that the storm warnings can be made even more in advance [20]. The solar radiation pressure would act oppositely to the gravitational attraction of the Sun. With this force cancelling effect, an orbit period identical to the Earth orbit but closer to the Sun will emerge. A sailcraft operating at this artificially-created Lagrange point upstream of the Earth is therefore a non-Keplerian orbit that cannot be obtained by conventional propulsion techniques.

I.2.2.   Attitude Analysis

Conventional methods of attitude control such as thrusters are an expensive solution to use on small sailcraft because they add complexity and mass to the system (thruster and propellant mass), and the need for propellant limits the mission duration. Wokes, et. al. selected

miniature thrusters to counteract disturbances on a large 245 m x 245 m solar sail [6]. However for a relatively small 40 m^2 sail, conventional thrusters are not an ideal solution. As compared with conventional spacecraft, significant solar thrust forces act on the sail. Many have proposed using simple sail-oriented devices that can manipulate this force and provide the necessary attitude control without carrying propulsive fuel.

Sail devices can alter the center of pressure and center of mass locations within the sailcraft system to give rise to control torques. Piggot, et. al. studied the use of four tip vanes (Figure 1) for attitude control [7]. The tip vane articulation can change the location of the center of pressure relative to the center of mass on the sail. This alters the forces on the sail and gives rise to torques. The tip vanes can be maneuvered in such a manner that will supply attitude control torques. Another attitude control technique uses the center of mass location change (instead of center of pressure) to provide the control torque. The sailcraft typically has a concentrated bus mass on the order of the mass of the sail. Thus, bus motion relative to the sail can produce significant changes in the location of the center of mass relative to the center of pressure. This center of pressure to center of mass (cp-cm) offset modifies the forces and thus results in torques on the sail. Wie, et. al. have utilized the motion of the sailcraft bus on a gimbaled boom to provide the necessary control torques [30]. Apart from a non-spinning square solar sail, Rizvi, et. al. have studied a spinning heliogyro that uses the sail blade pitching motion to alter the thrust forces on the sailcraft and produce the required control torques [21].

I.2.3.   *Structural Analysis*

In order to analyze solar sail attitude dynamics and control, accurate prediction of forces and moments acting on the sail are required. Most attitude control systems have been developed for a flat sail. An actual sail in orbit, however, billows out due to the solar radiation pressure.

Such sail deformation alters the center of mass to center of pressure offset and thus modifies the resultant thrust force and moment acting on the sail. In a research study, a geometrically nonlinear finite element method is used to calculate force and moment exerted on an arbitrarily shaped solar sail subjected to solar radiation pressure [24]. In addition, it is shown that sail deformation due to solar pressure load can be approximated by deformations that are caused by corresponding uniform gas pressure load. This facilitates force and moment sail analysis via commercial finite element codes. With improved sail structural dynamics, force and moment predictions, more accurate attitude controller designs can be developed.

Along with sail shape aberrations, sail surface quality degradation also affects sail attitude. Non-uniform sail reflective property and mass distribution give rise to unknown forces and moments to the control algorithms. A study to reveal how real, imperfect sails act as propulsion devices shows that surface quality errors result in an unacceptable mission profile when no initial calibration or on-the-fly corrections are made [3]. Thus, surface quality degradation prediction remains a difficult challenge.

Apart from sail shape deformation and surface defects, sail deployment is also a concern. A challenge has been to study how folded sail membranes behave when deployed. The spacecraft structure houses the creased and packed sail until deployed in space. There is interest in the use of thin-film membrane structures for future gossamer spacecraft missions such as solar sails. Ultrasail (light weight, spinning solar sail) design relies on thin films for propulsion. The structure does not contain booms or masts, which significantly reduces mass and enables high payload fractions and accelerations [1]. A different study on a 500 mm x 500 mm thin-film membrane determined the shape of the deployed membrane and load displacement relationship for in-plane, diagonal loading of the sail corners [19]. Although the analytical analysis is

applicable to larger, sail-size membranes, it still remains inconclusive for sail deployment in space because the space environment torques and forces are not simulated. NASA's advances in solar sail technology however simulated a more space-like environment. The NanoSail-D mission developed, deployed and conducted vacuum testing on two 20 m^2 solar sail systems [4]. Although the mission never reached Earth orbit due to launch vehicle failures, NASA achieved advances toward these missions to develop, build and ground-test an innovative solar sail satellite.

I.2.4.   *Inducing Orbit Effects via Sail Attitude Manipulation*

Orbit changes result from orienting the thrust vector with respect to the Sun, which requires the attitude of the sail to be controlled. Due to the large size of the sail, significant solar, aerodynamic and gravity gradient torques act on the sail and can disturb the sail attitude relative to the Sun. Accordingly, large control torques are needed to counteract these attitude disturbances, and an understanding of sail attitude dynamics is required in order to design appropriate control algorithms.

Recent studies have analyzed natural sail dynamics in order to maintain the desired thrust vector pointing [9 and 13]. Generally, large external torques are required to maintain the desired thrust vector pointing relative to the Sun. Lawrence, et. al. have shown that specific kinds of torques can be generated naturally under the influence of solar, aerodynamic and gravity gradient torques [9]. This reduces the need for expensive and massive traditional attitude control techniques (attitude jets or reaction wheels). The basic idea is to operate at the attitude equilibria of the sail normal vector in the local vertical local horizontal (LVLH) frame. An extension of this idea is to utilize a slight deviation of the sail normal from these equilibria, which results in sail

normal coning about that equilibrium. McMahon, et. al. have shown that any desired orbit changes can be obtained with sail normal coning at orbit rate (circular cones) [13].
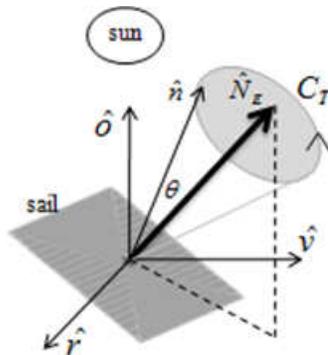
Figure 5: Sail Normal Coning in the Local Vertical Local Horizontal Frame

In Figure 5, the sail normal cones about the LVLH equilibrium attitude, $\hat{N}_E$. With a slight deviation, θ from the equilibrium attitude, the normal vector, $\hat{n}$ traces a coning trajectory, C_T in the L-frame (defines natural sail coning). The cone tracing should occur at orbit rate to attain desired sail orbit changes. Swartwout, et. al.'s sail steering law also produces the desired orbital effects, however with significant control torque and rapid maneuvers that can damage the sail [28]. In contrast, McMahon's approach produces smooth sail rotation rates that avoid disturbing the structural sail dynamics [13]. In his work, all ranges of the desired orbital effects can be attained when the natural sail coning occurs at orbit rate [13]. This thesis intends to build upon these studies and explore the feasibility of designing a control that can enable the sail normal to trace a circular coning trajectory at orbit rate.

II. SOLAR SAIL CONING

In this chapter, the dynamics of the solar sail are presented. With the sail dynamics, the concept of sail attitude equilibrium in the local vertical local horizontal frame (L-frame) is explained. The L-frame sail attitude equilibria enable sail normal coning in the inertial frame (A-frame). A small perturbation from the sail attitude equilibria induces L-frame coning of the sail normal about those sail equilibria. This L-frame coning of the sail is discussed in this chapter. It is shown that natural environmental torques can cause sail precession and enable L-frame sail coning.

Many orbital effects can be obtained due to the L-frame coning of the sail normal about the sail equilibria. However, the natural rate and shape of coning of the sail normal about the sail equilibrium point does not yield the desired orbital effects. Control torques can be used to enforce the desired rate and coning shape (circular cones). The use of control torque to enforce circular sail normal coning at the desired rate is the main subject of this chapter. The control torque magnitude is different based upon how fast the sail spins about its own axis (sail spin rate). The effects of variable sail spin rate on the required control torque are discussed. Finally, different sail spin rates are used in the sail simulation and results showing the coning of the sail normal in the L-frame about the sail equilibrium are presented.

II.1. *Dynamics of Spinning Solar Sails*

The sailcraft studied consists of a solar sail and sailcraft bus, which is located out of the sail plane. The sailcraft model used in this study is shown in Figure 6.
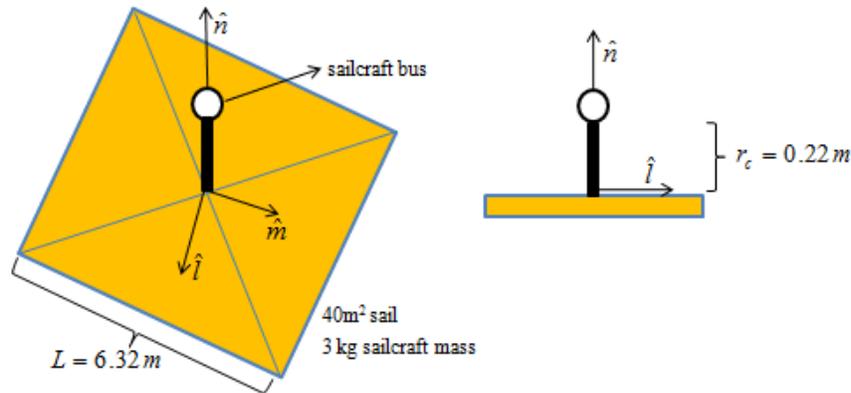
Figure 6: Physical Components and Dimensions of the Sailcraft Model

The sail is assumed to be flat, rigid, uniform, square with a sailcraft bus located out of the sail

plane at a distance r_c along the sail normal, $\hat{n}$. Since the sail is symmetric and rotation about $\hat{n}$

does not alter any solar, aerodynamic, or gravity gradient forces, the sail attitude can be

described only by the sail normal vector when considering these external effects. The bus is

located near the plane of the sail (0.22 m) as compared with the sail size (40 m^2), which enables

the sailcraft moment of inertia to be similar to that of a flat plat [22]. A large, gossamer sail will

be non-rigid in space. It is argued that the orbital element control applications using coning

motions produce smooth, low frequency environmental torques, on the order of orbit frequency

and require closed loop settling times on the order of several orbits. The disturbance frequencies

and control system bandwidths are on the order of 10^{-4} Hz (for 700 km Low Earth Orbit),

whereas the lowest structural modes of the sail are in the range of 10^{-1} to 10^{-2} Hz [5]. This

suggests that the torque applications do not excite the sail structural modes, thus justifying the

rigid body assumption from a control-structure interaction viewpoint. Non-uniform material

properties within the sail will cause imperfect solar reflections and variations in pressure-loading

on the sail. The varying pressure-loading issue will deform the sail and hence it will no longer

remain flat in orbit. A deformed sail will experience different torques as a function of attitude.

However, the varying pressure-loading issue is a secondary effect and offers more insight on the

sailcraft torque as a function of attitude by deviating from the ideal case. This thesis study focuses on the ideal (flat) case.

In order to describe the sail dynamics in a circular orbit, the reference frames used are given in Figure 7 [9].
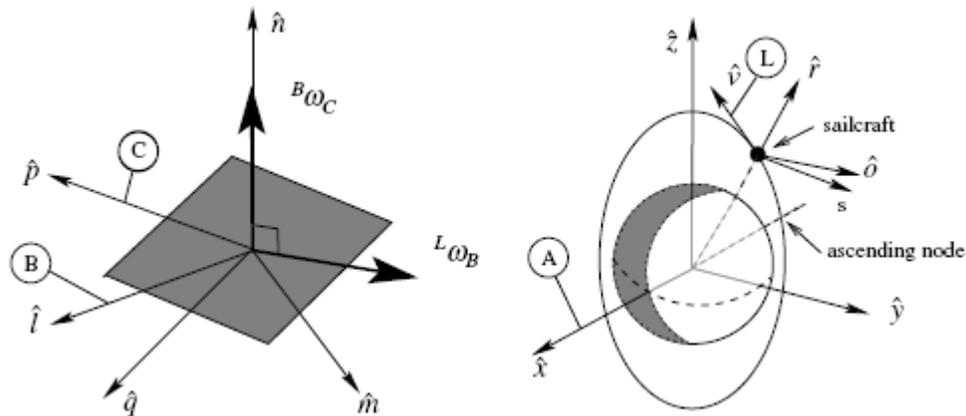
Figure 7: Reference Frames used to Develop Sail Dynamics[9]

The A-frame $\{\hat{x}, \hat{y}, \hat{z}\}$ is the inertial (fixed) frame. The $\hat{x}$ and $\hat{y}$ define the Earth equatorial frame with $\hat{x}$ pointing along the vernal equinox. The $\hat{z}$ is normal to the equatorial frame. The local vertical local horizontal or L-frame $\{\hat{r}, \hat{v}, \hat{o}\}$ rotates along with the orbit at orbit rate. The $\hat{r}$ points along the orbit radial direction, $\hat{v}$ is in the direction of the sail velocity vector and $\hat{o}$ is aligned with the orbit angular momentum. The C-frame $\{\hat{n}, \hat{p}, \hat{q}\}$ is the sail body-fixed frame. The $\hat{n}$ points along the sail normal vector (normal to the plane of the sail). The $\hat{p}$ and $\hat{q}$ remain in the plane of the sail. The B-frame $\{\hat{n}, \hat{l}, \hat{m}\}$ is also a body frame except that it does not rotate with the sail in the rotation about $\hat{n}$. The $\hat{l}$ and $\hat{m}$ lie in the plane of the sail. Thus, the only difference between the B-frame and C-frame is the rotation about $\hat{n}$. The B-frame is taken to be aligned with the C-frame at the initial time epoch.

The sailcraft dynamics are described by forming a relationship between the inertial angular momentum vector and torque on the sail. The inertial angular momentum vector in the C-frame as seen in the A-frame is

$$^A\vec{h}_C = I_s \cdot {}^A\vec{\omega}_C \tag{1}$$

where I_s and $^A\vec{\omega}_C$ are sail inertia tensor and inertial angular velocity. The change in $^A\vec{h}_C$ is caused by the application of net external torque on the sail.

$$^A\frac{d}{dt}{}^A\vec{h}_C = \vec{\tau} = {}^B\frac{d}{dt}{}^A\vec{h}_C + {}^A\vec{\omega}_B \times {}^A\vec{h}_C = I_s \cdot {}^B\frac{d}{dt}{}^A\vec{\omega}_C + {}^A\vec{\omega}_B \times \left(I_s \cdot {}^A\vec{\omega}_C\right) \tag{2}$$

The I_s is fixed in the B-frame because the B-frame is a principal frame due to the symmetry about $\hat{n}$. The B-frame is defined such that the relative angular velocity of the B-frame as seen in the L-frame, $^L\vec{\omega}_B$ is zero about $\hat{n}$ [9]. With this definition of the B-frame, the tip and tilt of the sail relative to the L-frame are described. The additional sail spin about $\hat{n}$ is not included in the B-frame. The advantage of creating a separation between the sail spin about $\hat{n}$ and the tip and tilt velocities ($^L\vec{\omega}_B$) about $\hat{n}$ is that the dynamics can be written in terms of the normal (along $\hat{n}$) and transverse (orthogonal to $\hat{n}$) components. The inertial spin about $\hat{n}$ is given by

$$\begin{aligned}
\omega_n &= \hat{n} \cdot {}^A\vec{\omega}_C = \hat{n} \cdot \left({}^A\vec{\omega}_L + {}^L\vec{\omega}_B + {}^B\vec{\omega}_C\right) = \omega_s + \omega_\perp \\
\omega_s &= \hat{n} \cdot {}^B\vec{\omega}_C \\
\omega_\perp &= \hat{n} \cdot {}^A\vec{\omega}_L = \omega_o \hat{o} \cdot \hat{n} \\
\hat{n} \cdot {}^L\vec{\omega}_B &= 0
\end{aligned} \tag{3}$$

where $^A\vec{\omega}_L$ is the orbit rate and $\hat{n} \cdot {}^L\vec{\omega}_B = 0$ follows from the definition of the B-frame. Now, $^A\vec{\omega}_B$ is partitioned as

$$\begin{aligned}
^A\vec{\omega}_B &= \vec{\omega}_T + \omega_\perp \hat{n} \\
\vec{\omega}_T &= \left(I - \hat{n} \cdot \hat{n}\right) {}^A\vec{\omega}_B
\end{aligned} \tag{4}$$

where $\vec{\omega}_T$ is the projection of $^A\vec{\omega}_B$ onto the plane described by $\hat{n}$. With these definitions,

$$
\begin{aligned}
I_s \cdot {}^A\vec{\omega}_C &= I_s \cdot \left({}^A\vec{\omega}_B + {}^B\vec{\omega}_C \right) = I_s \cdot \left(\vec{\omega}_T + \omega_\perp \hat{n} + \omega_s \hat{n} \right) = I_s \cdot \left(\vec{\omega}_T + \omega_n \hat{n} \right) = I_T \vec{\omega}_T + I_n \omega_n \hat{n} \\
{}^A\vec{\omega}_B \times \left(I_s \cdot {}^A\vec{\omega}_C \right) &= \left(\vec{\omega}_T + \omega_\perp \hat{n} \right) \times \left(I_T \vec{\omega}_T + I_n \omega_n \hat{n} \right) = \left(\omega_n I_n - \omega_\perp I_T \right) \vec{\omega}_T \times \hat{n}
\end{aligned}
\tag{5}
$$

where I_T and I_n are transverse and axial moment of inertias. Now, equation 2 results in the sail dynamics in terms of the transverse and normal components.

$$
\begin{aligned}
\vec{\tau} &= I_s \cdot {}^B\frac{d}{dt}\left(\vec{\omega}_T + \omega_n \hat{n} \right) + {}^A\vec{\omega}_B \times \left(I_s \cdot {}^A\vec{\omega}_C \right) \\
\vec{\tau}_T &= I_T \cdot {}^B\frac{d}{dt}\vec{\omega}_T + \left(\omega_n I_n - \omega_\perp I_T \right) \vec{\omega}_T \times \hat{n} \\
\vec{\tau}_n &= I_n \cdot \dot{\omega}_n \hat{n}
\end{aligned}
\tag{6}
$$

The derivation of the normal and transverse components of the sail dynamics can also be found in Lawrence, et. al. [13].

II.2. Sail Equilibria in the L-frame and Inertial Sail Normal Coning

Any fixed sail normal $\hat{n}$ in the L-frame describes the sail equilibrium attitude in the L-frame. The sail attitude can be defined by the sail normal vector, $\hat{n}$ because the sail is symmetric about $\hat{n}$ and the rotation about $\hat{n}$ does not alter the forces on the sail. When the sail normal, $\hat{n}$ is fixed in the L-frame, but not aligned with $\hat{o}$, the sail rotates with the orbit and produces inertial coning of $\hat{n}$ at orbit rate.
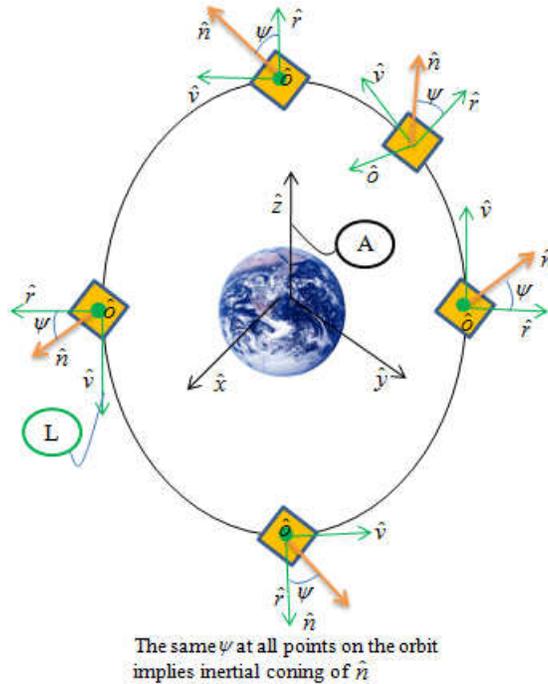
Figure 8: Illustration of Inertial Coning of the L-frame Fixed Sail Normal

In Figure 8, the sail normal remains fixed in the L-frame (indicated by the constant angle ψ) and causes inertial coning of $\hat{n}$ at orbit rate. By choosing ψ appropriately, the sail angular momentum precesses to provide inertial coning with desirable orbit change effects. The angular momentum precession, in turn, is caused by torques acting on the sail. To obtain the desired angular momentum precession, the required torques on the sail must be determined.

For $\hat{n}$ to remain fixed in the L-frame and enable inertial coning, the sail angular momentum must precess at a desired rate. The $^{L}\vec{\omega}_{B} = 0$ because there is no tip and tilt of $\hat{n}$ relative to the L-frame ($\hat{n}$ is fixed in the L-frame). In addition, B-frame is also fixed in the L-frame by the definition of the B-frame $\left(^{L}\vec{\omega}_{B} \cdot \hat{n} = 0 \right)$ and thus

$$\begin{aligned} ^{A}\vec{\omega}_{B} &= {}^{A}\vec{\omega}_{L} + {}^{L}\vec{\omega}_{B} = {}^{A}\vec{\omega}_{L} \\ \frac{^{B}d}{dt} {}^{A}\vec{\omega}_{B} &= \frac{^{L}d}{dt} {}^{A}\vec{\omega}_{L} = \frac{^{L}d}{dt} \omega_{o}\hat{o} = 0 \end{aligned} \qquad (7)$$

since $\hat{o}$ is fixed in the L-frame and the orbit rate, ω_o is assumed to be a constant (because the sail

force changes the semi-major axis, and hence the orbit period slowly as compared to the sail

attitude motions). With $\dfrac{^B d}{dt}{}^A\vec{\omega}_B = 0$

$$\frac{^B d}{dt}\vec{\omega}_T = \frac{^B d}{dt}(I - \hat{n}\hat{n})^A\vec{\omega}_B = \frac{^B d}{dt}\left({}^A\vec{\omega}_B\right) - \frac{^B d}{dt}\left({}^A\vec{\omega}_B \cdot \hat{n}\right)\hat{n} = -\frac{^B d}{dt}\left({}^A\vec{\omega}_L \cdot \hat{n}\right)\hat{n} = -\frac{^L d}{dt}(\omega_o\hat{o} \cdot \hat{n})\hat{n} = 0 \quad (8)$$

since $\hat{o}$ and $\hat{n}$ are fixed in the L-frame. Now, the torques orthogonal to $\hat{n}$ become

$$\vec{\tau}_T = (\omega_n I_n - \omega_\perp I_T)\vec{\omega}_T \times \hat{n} \tag{9}$$

From the control viewpoint, the sail spin rate ω_s must remain a constant. A constant ω_s avoids

any abrupt and impractical changes in the sail spin rate that can damage the sail. Since

$\omega_n = \omega_s + \omega_\perp$ and $\omega_\perp$ is a constant ($\omega_\perp = \omega_o\hat{o} \cdot \hat{n}$: sail attitude, $\hat{n}$ and $\hat{o}$ are fixed in the L-frame

and ω_o is a constant) then for ω_s to remain a constant, ω_n also has to be a constant. The ω_n can

remain a constant when the torque along $\hat{n}$ is zero.

$$\vec{\tau}_n = I_n \cdot \dot{\omega}_n\hat{n} = 0 \rightarrow \dot{\omega}_n = 0 \tag{10}$$

Now, ${}^A\vec{\omega}_C = {}^A\vec{\omega}_L + \omega_s\hat{n}$ and

$$\frac{^B d}{dt}{}^A\vec{\omega}_C = \frac{^L d}{dt}\left({}^A\vec{\omega}_L + \omega_s\hat{n}\right) = \frac{^L d}{dt}\omega_s\hat{n} = 0 \tag{11}$$

because ω_s is a constant and $\hat{n}$ is fixed in the L-frame. The sail normal $\hat{n}$ can be described in the L-frame via a cone angle β and a clock angle ϕ.
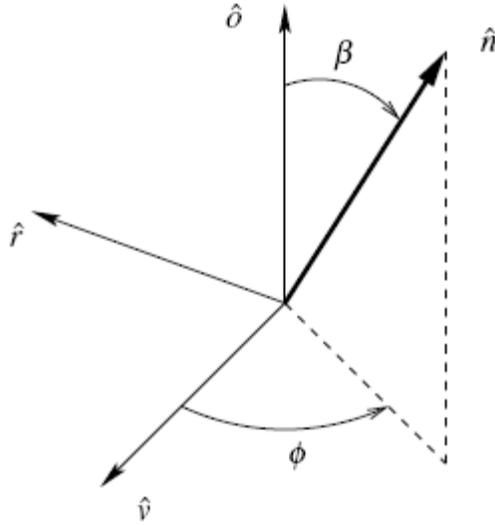
Figure 9: Cone and Clock Angles of the Sail Normal relative to the L-frame[9]

From Figure 9 [9], the sail normal, $\hat{n}$ becomes

$$\hat{n} = -(\sin\beta\sin\phi)\hat{r} + (\sin\beta\cos\phi)\hat{v} + (\cos\beta)\hat{o} \tag{12}$$

With this definition of $\hat{n}$

$$\begin{aligned}
\omega_{\perp} &= \omega_o\hat{o}\cdot\hat{n} = \omega_o\cos\beta \\
\vec{\omega}_T &= (I - \hat{n}\hat{n})^A\vec{\omega}_B = (I - \hat{n}\hat{n})\cdot\left(^A\vec{\omega}_L + ^L\vec{\omega}_B\right) = (I - \hat{n}\hat{n})\cdot\omega_o\hat{o} = \omega_o(\hat{o} - \cos\beta\cdot\hat{n}) \\
\vec{\omega}_T \times \hat{n} &= -\omega_o\sin\beta\cdot(\cos\phi\hat{r} + \sin\phi\hat{v})
\end{aligned} \tag{13}$$

Thus, for $\hat{n}$ and ω_s to remain fixed in L, the normal and transverse torques must satisfy

$$\begin{aligned}
\vec{\tau}_T &= -(\omega_n I_n - \omega_o I_T \cos\beta)\cdot\omega_o\sin\beta\cdot(\cos\phi\hat{r} + \sin\phi\hat{v}) \\
\vec{\tau}_n &= \vec{0}
\end{aligned} \tag{14}$$

These are the required torques that will enable the desired sail angular momentum precession for the inertial coning of the sail normal in the A-frame. According to Lawrence, et. al., the environmental torques acting on the sail can provide the necessary torques for such sail attitude equilibria to exist in the L-frame and have inertial sail coning [9], as discussed in more detail below.

II.3.   *Environmental Torques*

In order to attain a fixed orientation of $\hat{n}$ in the L-frame, a balance between the torques acting on the sail and precession of the sail angular momentum is required. Apart from control torques, the natural environmental torques acting on the sail are the aerodynamic, solar pressure and gravity gradient torques. The aerodynamic and solar pressure torques produce negligible forces in conventional spacecraft. However, due to the large sail area, the forces emerging from the aerodynamic and solar pressure torques are greatly magnified in the sailcraft. In addition, the sailcraft has significant gravity gradient torques because its mass properties resemble that of a flat plate. Lawrence, et. al. propose that the desired inertial coning of the sail normal can be attained by advantageously employing these environmental torques with the natural spin dynamics of the sail [9]. The sailcraft is spun at a specific rate such that the aerodynamic, solar pressure and gravity gradient torques provide the desired precession of the momentum vector and thus induce inertial coning of $\hat{n}$.

The aerodynamic torque, $\vec{\tau}_a$ on the sailcraft depends on the orientation of $\hat{n}$ relative to the aerodynamic force vector, which is approximately in the direction of the sailcraft velocity vector, $\hat{v}$.

$$\vec{\tau}_a = -\tau_{am} \sin\beta|\cos\phi|(\cos\beta\hat{r} + \sin\beta\sin\phi\hat{o})$$
$$\tau_{am} = \frac{1}{2}r_{cp-cm}\rho C_D v^2 A$$

(15)

where τ_{am} is the aerodynamic moment coefficient for a given cp-cm offset r_{cp-cm}, atmospheric density ρ, coefficient of drag C_D, sailcraft velocity v relative to the atmosphere and sail area A. The solar torque, $\vec{\tau}_s$ depends on the orientation of $\hat{n}$ relative to the sailcraft Sun vector, $\hat{s}$ (assume that the Sun vector is in the orbit normal direction, $\hat{s} = \hat{o}$).

$$\vec{\tau}_s = \tau_{sm} \sin\beta |\cos\beta| (\cos\phi\hat{r} + \sin\phi\hat{v})$$
$$\tau_{sm} = r_c (1 - f_s) PA \tag{16}$$

where τ_{sm} is the solar moment coefficient for a given solar pressure, P and specular reflectance

fraction, f_s. The gravity gradient torque, $\vec{\tau}_g$ is given by

$$\vec{\tau}_g = 3\tau_{gm} \sin\beta \sin\phi (\cos\beta\hat{v} - \sin\beta\cos\phi\hat{o})$$
$$\tau_{gm} = \omega_o^2 (I_n - I_T) \tag{17}$$

where τ_{gm} is the gravity moment coefficient that depends on sailcraft mass properties and orbit

rate.

II.4. *Torque Balance to Attain Sail Equilibria in the L-frame*

The net torque, $\vec{\tau} = \vec{\tau}_a + \vec{\tau}_s + \vec{\tau}_g$ must satisfy equation 14 and yield the required torques to

provide inertial coning of $\hat{n}$ and thus fixed attitude in the L-frame. Three simultaneous equations

emerge, creating a balance between the net torque, $\vec{\tau}$ and required torque (equation 14).

$$\hat{r} \rightarrow -(\omega_{no}I_n - \omega_o I_T \cos\beta)\cdot\omega_o \sin\beta\cos\phi = -\tau_{am} \sin\beta\cos\beta|\cos\phi| + \tau_{sm} \sin\beta|\cos\beta|\cos\phi$$
$$\hat{v} \rightarrow -(\omega_{no}I_n - \omega_o I_T \cos\beta)\cdot\omega_o \sin\beta\sin\phi = \tau_{sm} \sin\beta|\cos\beta|\sin\phi + 3\tau_{gm} \sin\beta\cos\beta\sin\phi \tag{18}$$
$$\hat{o} \rightarrow 0 = -\tau_{am} \sin^2\beta|\cos\phi|\sin\phi + 3\tau_{gm} \sin^2\beta\cos\phi\sin\phi$$

where ω_{no} corresponds to the equilibrium sail spin that the sail must maintain in order to provide

the required torques (to satisfy the three components of equation 18). Thus, a given β and ϕ

orientation of $\hat{n}$ in the L-frame is an equilibrium solution to the sail attitude dynamics when a spin

rate ω_{no} exists and satisfies the three equations for arbitrary values of $\tau_{am}, \tau_{sm}, \omega_o$ (orbit

parameters), I_n and I_T (sailcraft design parameters). The equilibrium cases that emerge due to

relationships between $\tau_{am}, \tau_{sm}, \omega_o, I_n$ and I_T are excluded because these would restrict the orbit

and sailcraft properties and make the mission impractical. Thus, the sail spin rate is treated as a

variable to reach equilibrium. There are two types of equilibria points explored in this thesis because they were found to be neutrally stable equilibria [9] and produced orbit lowering/raising (a typical application of solar sails).

1. $\phi = 0°$: causes orbit lowering by producing a component of solar thrust vector in the anti-velocity direction. The equilibrium spin rate required is

$$\omega_{no} = \frac{\cos \beta}{I_n \omega_o} \left(\omega_o{}^2 I_T + \tau_{am} - \tau_{sm} sign(\cos \beta) \right) \qquad (19)$$

2. $\phi = \pi$: causes orbit raising by producing a component of solar thrust vector in the velocity direction. The required equilibrium spin rate is

$$\omega_{no} = \frac{\cos \beta}{I_n \omega_o} \left(\omega_o{}^2 I_T - \tau_{am} - \tau_{sm} sign(\cos \beta) \right) \qquad (20)$$

Simulation results for one of these equilibrium points are presented in the following section.

II.5. CubeSail Simulation

Lawrence, et. al. have created a MATLAB simulation for a CubeSail (small solar sail satellite) that propagates the sailcraft attitude under the influence of aerodynamic, solar pressure and gravity gradient torques over a circular, Low Earth Orbit [9]. The orbit and sailcraft parameters used are shown in Table 1.

Table 1: Orbit and Sailcraft Parameters

Orbit Parameters	
Altitude, a	700 km
Inclination, i	90°
Right ascension of ascending node, Ω	180°
Orbit rate, ω_o	1.06 x 10^{-3} rad/s
Right ascension of sun, r_s	90°
Declination of sun, d_s	0°
Solar flux at 1 AU, F_s	1358 W/m^2
Atmospheric density, ρ	5 x 10^{-14} kg/m^3
Aerodynamic moment coefficient, τ_{am}	1.18 x 10^{-5} Nm
Solar moment coefficient, τ_{sm}	9.84 x 10^{-6} Nm
Gravity gradient moment coefficient, τ_{gm}	6.33 x 10^{-6} Nm
Sailcraft Parameters	
Sail side length, L	6.325 m
Sail mass, m_s	1.7 kg
Sailcraft bus mass, m_b	1.3 kg
Distance to bus from sail plane in $\hat{n}$ direction, r_c	0.22 m
Axial moment of inertia, I_n	11.3 kgm^2
Transverse moment of inertia, I_t	5.7 kgm^2
Sail reflectivity, s	0.9
Aerodynamic coefficient of drag, C_d	2.2
Specular reflectance fraction, f_s	0.7

Along with these parameters, for a cone angle of $\beta_0 = 35°$ and clock angle of $\phi_0 = 0°$ (ω_{no} was calculated to be 6.32 x 10^{-4} rad/s), the simulation was run for two orbital periods. Figure 10 shows the results for the motion of the sail normal, $\hat{n}$ in the L-frame.
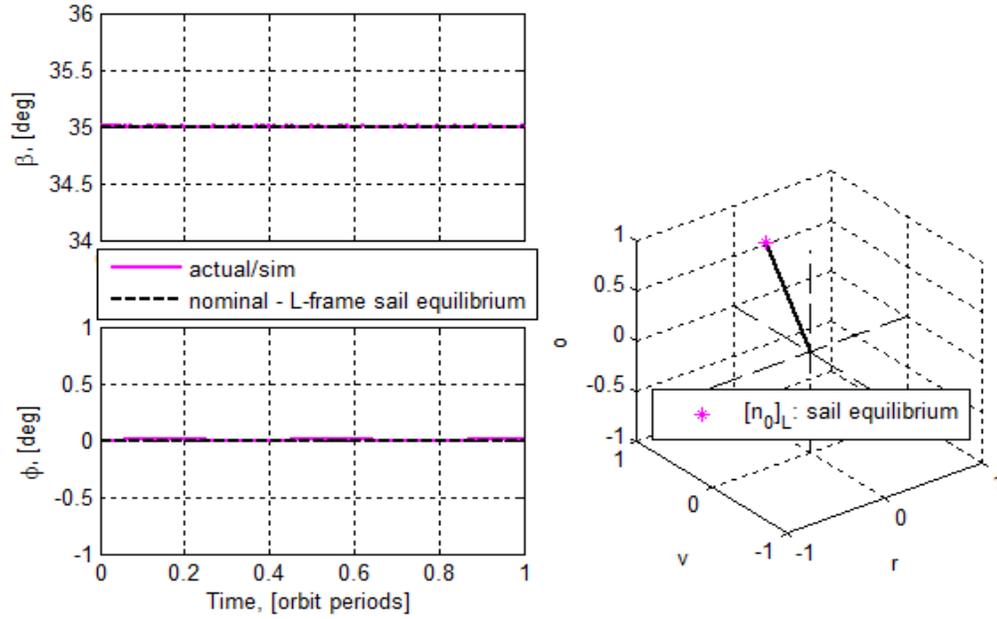
Figure 10: Sail Equilibrium in the L-frame (Sail Normal is Fixed in the L-frame)

The β and ϕ angles along with the $\hat{n}$ stay fixed in the L-frame. Figure 11 shows the results for the motion of $\hat{n}$ in the A-frame.
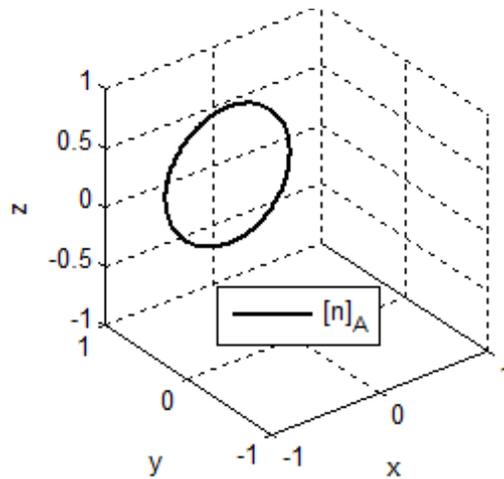

Figure 11: Inertial Coning of the Sail Normal in the A-frame

Observe that $\hat{n}$ is fixed in the L frame, but exhibits inertial coning (in the A-frame).

II.6.   L-frame Sail Normal Coning

Lawrence, et. al. have shown that for the developed sail dynamics, a small sail normal perturbation from the L-frame attitude equilibrium enables the sail normal to cone about that equilibrium point [9]. This constitutes sail normal coning in the L-frame illustrated in Figure 12.
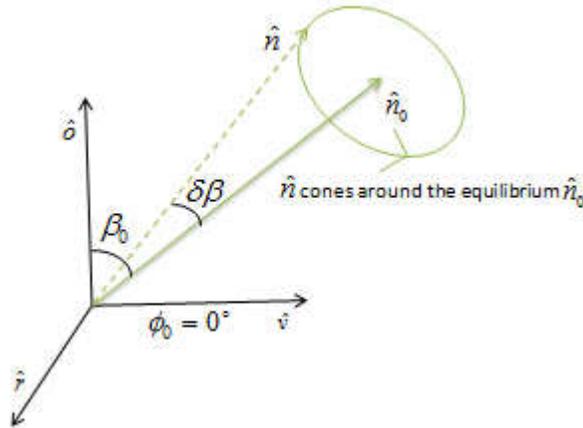

Figure 12: Illustration of the Sail Normal Coning in the L-frame

The $\hat{n}_0$ exhibits the sail equilibrium point and $\hat{n}$ is the coning sail normal vector. The perturbation is given by a small deviation, $\delta\beta$ in the cone angle, β. The coning is defined such that the cone need not be circular or have a fixed coning rate. As discussed earlier, McMahon, et. al. have shown that desired orbital effects can be induced when the L-frame coning occurs at orbit rate such that one rotation of $\hat{n}$ around $\hat{n}_0$ is completed in one orbital period and has a circular coning shape [13].

II.7.   Orbital Effects from L-frame Sail Normal Coning

McMahon, et. al. have analyzed the special case of circular coning of $\hat{n}$ about a stable equilibrium attitude in the L-frame [13]. Neutrally stable equilibria are considered because small perturbations from the equilibrium does not allow $\hat{n}$ to asymptotically increase away from or decrease towards the equilibrium point. Thus, a natural coning motion is exhibited. When one

coning rotation is completed per orbit, nearly any orbital effect can be induced with zero control torque and minimal excitation of structural dynamics (due to the smooth coning motions). As a special case, operating at the sail equilibrium attitude (and not cone about the attitude) the induced orbital effects are restricted to orbit raising and lowering.

When the coning motion is implemented, changes in the orbital angular momentum vector, energy and eccentricity vector emerge. The orbital effects that are induced via the coning motions can have many applications. One application is for Sun-synchronous orbits, where the orbit right ascension of ascending node must drift at a required rate for the spacecraft to remain Sun-synchronous. The nodal drift is naturally caused by the J_2 gravitational effect and is a function of orbit radius, inclination and eccentricity. With the proper coning motion of $\hat{n}$, the solar sail can be used to overcome undesired nodal drift from errors in the semi-major axis (orbit radius and eccentricity) and inclination. In addition, the solar sail can also be used to provide additional nodal drift and thus create new Sun-synchronous orbits which are not possible with just the J_2 effect. Another application of the coning motion is to use the solar sail to overcome injection error from the launch. McMahon, et. al. have shown that the launch errors from the Pegasus, Delta II, Delta IV, Atlas V, Falcon I, Minotaur I and IV, and Taurus launch vehicles for Low Earth Orbits could be overcome by a solar sail [13].

II.8.   *Inducing L-frame Sail Normal Coning*

To attain sail equilibria in the L-frame and enable inertial sail coning, the sail angular momentum must achieve the desired precession rate. For the desired precession rate, the sail must spin about its axis at a required rate. The sail spin about its axis is described in Figure 13.
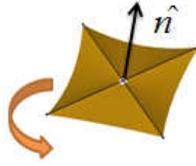
Figure 13: Sail Spin about the Sail Normal Vector

The desired sail spin rate will be referred to as the equilibrium sail spin rate. The equilibrium spin rates (ω_{no}) required for the sail attitude equilibria used in this study are given in equations 19 and 20. As the sail normal precesses from the equilibrium point and cones in the L-frame, the sail need not spin at the equilibrium rate. The control torques required to remain on the desired coning trajectory differ based upon the sail spin rate used. In order to minimize costs, the sail spin rate requiring the least control torque magnitude needed to trace the desired orbit rate circular coning trajectory should be used. The control torque induces the desired coning and enforces orbit rate coning. The part of the control torque used to induce the desired coning (referred to as coning control torque) allows the sail normal to trace the desired shape of the coning trajectory, whereas the other part of the control torque enforcing orbit rate coning (called as the rate control torque) allows the sail normal to trace the trajectory at the desired rate. The total control torque required to attain the desired orbit rate circular coning is a combination of these two control torques. When the sail normal is precessed from the attitude equilibrium and has the equilibrium sail spin rate, Lawrence, et. al. have shown that the sail normal exhibits natural coning about that sail equilibrium in the L-frame [9]. Due to the already coning behavior of the sail normal, the coning control torque magnitude is reduced. The natural coning motion does not occur at the desired orbit rate [9]. In order to enforce the coning at orbit rate, the magnitude of the rate control torque increases for the equilibrium sail spin case. This is because the spinning sail adds to the total angular momentum of the sailcraft and thus increases the rate control torque required to provide the desired momentum precession. As the sail spin rate

magnitude is reduced however, the sail does not carry as much momentum due to which the momentum can be precessed more easily with reduced rate control torque. On the other hand, deviations from the equilibrium spin rate can cause loss of natural coning behavior. This increases the need to require more coning control torque such that the desired coning motion can be attained. The rate control torque magnitude is the least for the zero sail spin rate because a non-spinning sail adds no additional momentum to the sailcraft momentum. This makes the desired momentum precession possible with the least rate control torque. Conversely, the coning control torque magnitude is the least for the equilibrium sail spin rate because the already coning behavior (natural coning) is best attained when the sail spins at the equilibrium rate. Due to this trade-off between the rate control torque and coning control torque (combination of both yields the total required control torque), it is interesting to study which sail spin rate can result in the desired orbit rate circular coning with the least control torque magnitude. In this thesis, the L-frame sail coning is analyzed for two sail spin rates: equilibrium spin rate and zero spin rate. Before determining the required control torques needed to enforce the desired coning, it is important to study the natural motion of the sail with the equilibrium and zero sail spin rates under the influence of the environmental (natural) torques. In the CubeSail simulation, a small perturbation ($\delta\beta = 1°$) is added to a sail equilibrium having a cone angle, $\beta = 35°$ and clock angle, $\phi = 0°$ (the significance of choosing this equilibrium point is explained in III.2).The simulation results showing the coning of $\hat{n}$ in the L-frame for these two spin rates are presented.
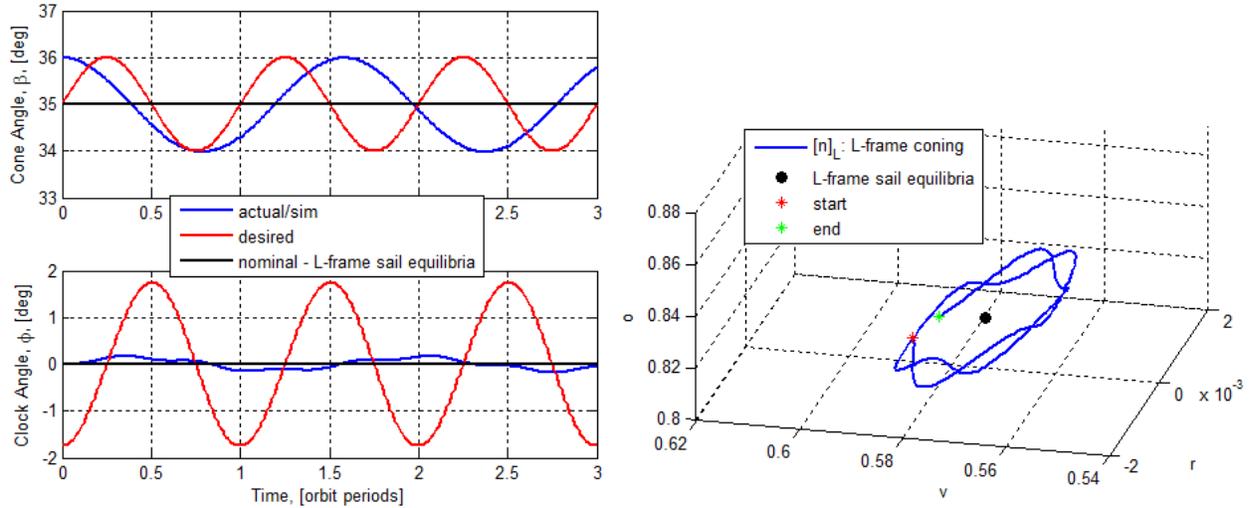
Figure 14: Sail Normal Coning in the L-frame about the Equilibrium Point, [β=35°, φ=0°] Using the Equilibrium Sail Spin Rate

The three-dimensional plot shows the motion of $\hat{n}$ in the L-frame. The two-dimensional plot gives a time history of the cone and clock angles over the course of several orbital periods. The $\hat{n}$ cones about the equilibrium point in the L-frame. However, the coning does not occur at orbit rate (one cone is traced in one and a half orbits).
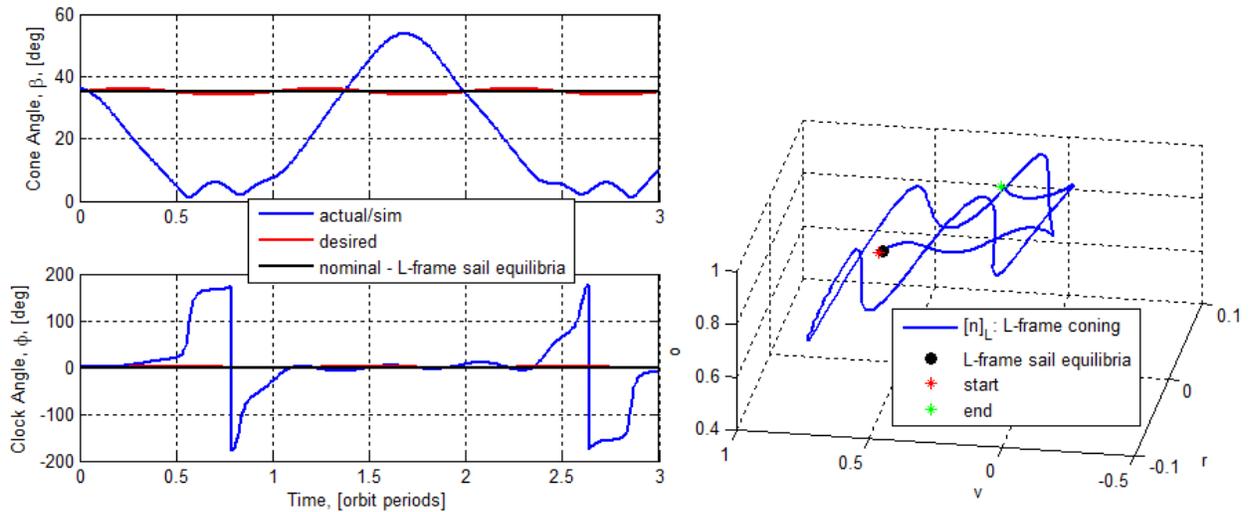

Figure 15: Sail Normal Coning in the L-frame about the Equilibrium Point, [β=35°, φ=0°] Using Zero Sail Spin Rate

Even though $\hat{n}$ stays in the vicinity of the equilibrium point, the coning is not well-defined in Figure 14. Since the sail is not spinning about $\hat{n}$ at the equilibrium spin rate (has zero sail spin),

the dynamics are different, and recognizable L-frame coning is not observed. Although quasi-periodic, the motion of $\hat{n}$ in the L-frame does not occur at orbit rate (one cone is traced every two orbits in this case).

Since the natural motion is not orbit rate circular coning (desired for useful orbital effects) control torques on the sailcraft are necessary. This thesis addresses the type of control method that can be used in order to enforce orbit rate circular coning and analyzes its performance. As Figures 13 and 14 suggest, control torque magnitude required to attain orbit rate circular coning will differ based upon the sail spin rate. In the case with equilibrium spin, more torque is required to precess the angular momentum desirably (due to the large angular momentum), but less is required to initiate the desired coning since the natural sail motion is already coning. In the case with zero spin, more torque will be required to attain the desired coning because the natural coning is not well-defined, but less is required to precess the angular momentum as there is only the angular momentum due to orbit rate rotation of the sailcraft. The amount of control torque required and which sail spin rate uses the least torque magnitude will also be explored in this thesis.

III. CONTROL METHOD

A control method is developed to enable the sail normal $\hat{n}$ to track the desired sail normal $\hat{n}_c$ on the circular coning trajectory and provide orbit rate coning in the L-frame. The control law must establish a relationship between the control torque, $\tau_{control}$ and sail motion $\hat{n}$ relative to the desired $\hat{n}_c$ that provides closed loop stability. Note that the sail angular momentum, $\vec{h}$ and $\tau_{control}$ are related by the simple dynamics $^{inertial}\left[\dot{\vec{h}}\right] = \tau$. Thus, a control method will be developed such that $\vec{h}$ tracks the desired angular momentum, $\vec{h}_c$ on the coning trajectory at orbit rate. The control law is used to reduce the error between $\vec{h}$ and $\vec{h}_c$. Since sail angular momentum is a function of sail normal/angular position (equation 32), the control law is created with the hope that error reduction in angular momentum and thus tracking the desired angular momentum at orbit rate will also lead to tracking the desired sail angular position at orbit rate (enable $\hat{n}$ to track $\hat{n}_c$).

III.1. *Angular Momentum Error Reduction Control Method Theory*

This control method enables the sail angular momentum vector $\vec{h}_S$ to trace the sail angular momentum vector on the desired circular coning trajectory $\vec{h}_c$ at orbit rate. This in-turn can cause the sail normal vector, $\hat{n}$ to trace the desired normal, $\hat{n}_c$ and hence yield the desired circular coning at orbit rate. Here $\vec{h}_S$ is the simplified notation for the angular momentum vector of the C-frame as seen by the A-frame (given as $^A\left[\vec{h}_S\right]_C$). Likewise, $\vec{h}_c$ is the simplified notation for the desired angular momentum vector of the C-frame as seen by the A-frame (given as $^A\left[\vec{h}_c\right]_C$). In

order to prescribe $\vec{h}_c$ the kinematics of the coning trajectory are calculated. For a given β_0 and ϕ_0,
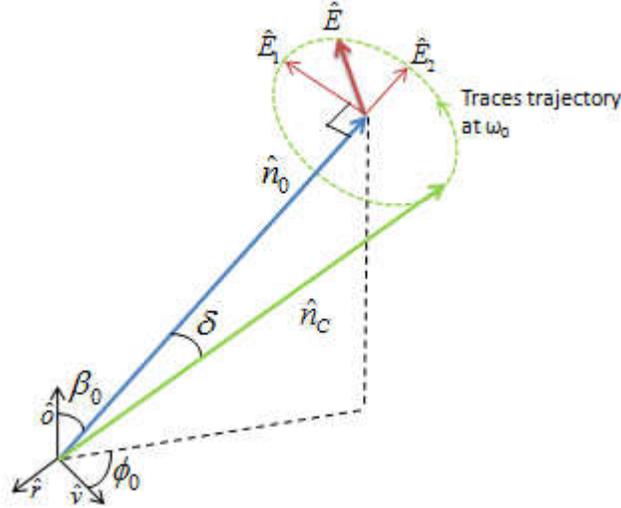
the desired coning trajectory is illustrated in Figure 16.

Figure 16: Desired Coning Trajectory

The desired trajectory traces a circular cone (half cone angle, δ) about nominal sail normal $\hat{n}_0$ at

orbit rate ω_o. The cone lies in a plane perpendicular to $\hat{n}_0$. The sail normal position on the cone at

each time step is given by $\hat{n}_c$. The motion of the sail normal $\hat{n}_c$ is determined by rotating $\hat{n}_0$ via a

time-varying rotation matrix, R_c^0 which has rotation axis $\hat{E}$ and rotation angle δ. In order to

calculate $\hat{E}$, a vector, $\hat{E}_1$ perpendicular to $\hat{n}_0$ is defined in the L-frame components.

$$\hat{E}_1 \perp \hat{n}_0 \rightarrow \left[\hat{E}_1\right]_L = \begin{bmatrix} \cos(\beta_0) \cdot \sin(\phi_0) \\ -\cos(\beta_0) \cdot \cos(\phi_0) \\ \sin(\beta_0) \end{bmatrix} \qquad (21)$$

A plane can be defined by two orthogonal vectors. Along with $\hat{E}_1$, the plane of the cone is

determined by calculating another vector, $\hat{E}_2 = \hat{E}_1 \times \hat{n}_0$. Now, the vector $\hat{E}$ at each time step can

be expressed as a linear combination of $\hat{E}_1$ and $\hat{E}_2$ in the plane of the cone.

$$\hat{E} = \cos(\omega_0 t) \cdot \hat{E}_1 + \sin(\omega_0 t) \cdot \hat{E}_2 \qquad (22)$$

With the rotation axis, $\hat{E}$ and defined rotation angle, δ, the rotation matrix, R_c^0 is [26]

$$R_c^0 = \cos(\delta) \cdot I_{3x3} + (1 - \cos\delta) \cdot \begin{bmatrix} \hat{E}(1)^2 & \hat{E}(1) \cdot \hat{E}(2) & \hat{E}(1) \cdot \hat{E}(3) \\ \hat{E}(1) \cdot \hat{E}(2) & \hat{E}(2)^2 & \hat{E}(2) \cdot \hat{E}(3) \\ \hat{E}(1) \cdot \hat{E}(3) & \hat{E}(2) \cdot \hat{E}(3) & \hat{E}(3)^2 \end{bmatrix} + \sin(\delta) \cdot \begin{bmatrix} 0 & \hat{E}(3) & -\hat{E}(2) \\ -\hat{E}(3) & 0 & \hat{E}(1) \\ \hat{E}(2) & -\hat{E}(1) & 0 \end{bmatrix} \quad (23)$$

and the sail normal, $\hat{n}_c$ is given by $\hat{n}_c = R_c^0 \cdot \hat{n}_0$. Using the definition of the sail normal in the L-frame, the desired angular position (β_c and ϕ_c) of the sail at each time step on the coning trajectory can be computed as

$$[\hat{n}_c]_L = \begin{bmatrix} -\sin(\beta_c) \cdot \sin(\phi_c) \\ \sin(\beta_c) \cdot \cos(\phi_c) \\ \cos(\beta_c) \end{bmatrix} \Rightarrow \begin{matrix} \beta_c = \cos^{-1}(\hat{n}_c(3)) \\ \phi_c = \tan^{-1}\left(\dfrac{-\hat{n}_c(1)}{\hat{n}_c(2)}\right) \end{matrix} \quad (24)$$

Figure 17 presents an example of the desired circular coning trajectory (half cone angle, $\delta = 1°$) throughout one orbital period for a given sail equilibrium point at $\beta_0 = 35°$ and $\phi_0 = 0°$.

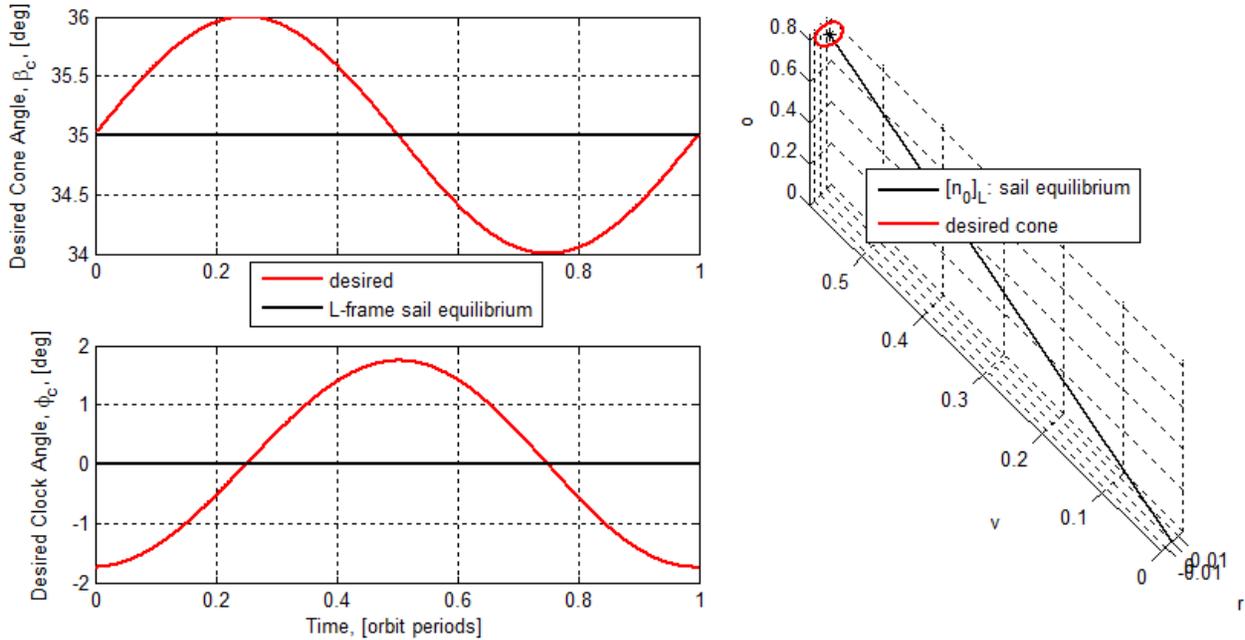Figure 17: Desired Circular Coning Trajectory having Half Cone Angle, δ=1° about a Nominal Sail Normal of β₀=35°, Φ₀=0° (One Orbital Period)

The nominal sail normal $\hat{n}_0$ is rotated at each time step with R_c^0 to yield the desired cone given by

$\hat{n}_c$. The β_c and ϕ_c of the coning motion (extracted from $\hat{n}_c$) exhibit sinusoidal behavior and can be

expressed as

$$\beta_c = \beta_0 + x \cdot \sin(\omega_0 \cdot t), x = \delta$$

$$\phi_c = y \cdot \cos(\omega_0 \cdot t), y = \tan^{-1}\left(\frac{-\hat{n}_c(1)_{time=0}}{\hat{n}_c(2)_{time=0}}\right) \tag{25}$$

From the desired angular position, the desired angular position rate ($\dot{\beta}_c$ and $\dot{\phi}_c$) is determined.

$$\dot{\beta}_c = \delta \cdot \omega_0 \cdot \cos(\omega_0 \cdot t)$$

$$\dot{\phi}_c = -y \cdot \omega_0 \cdot \sin(\omega_0 \cdot t), y = \tan^{-1}\left(\frac{-\hat{n}_c(1)_{time=0}}{\hat{n}_c(2)_{time=0}}\right) \tag{26}$$

The rate also has sinusoidal motion. Along with the desired angular positions and rates, the

desired angular velocity ($^L\vec{\omega}_B{}^*$) is also required to derive the kinematics of the coning trajectory.

The rate of change of $\hat{n}_c$ in the L-frame is

$$^L\frac{d\hat{n}_c}{dt} = {}^B\frac{d\hat{n}_c}{dt} + {}^L\vec{\omega}_B \times \hat{n}_c \rightarrow \frac{d[\hat{n}_c]_L}{dt} = [{}^L\vec{\omega}_B]_L \times [\hat{n}_c]_L \tag{27}$$

since the sail normal is fixed in the B-frame. The B-frame is defined such that the motion of $\hat{n}$ in

the L-frame only describes the sail tip and tilt velocities (there is no rotation about the $\hat{n}$

direction). Hence, equation 27 can define only two velocity components uniquely. Let the

angular velocity components of $^L\vec{\omega}_B$ in the L-frame be

$$[{}^L\vec{\omega}_B]_L = \begin{bmatrix} \omega_r \\ \omega_v \\ \omega_o \end{bmatrix}$$

Now $\dfrac{d[\hat{n}_c]_L}{dt}$ can be expanded as

$$\frac{d[\hat{n}_c]_L}{dt} = \begin{bmatrix} -\sin\beta_c \cos\phi_c \dot{\phi}_c - \cos\beta_c \sin\phi_c \dot{\beta}_c \\ -\sin\beta_c \sin\phi_c \dot{\phi}_c + \cos\beta_c \cos\phi_c \dot{\beta}_c \\ -\sin\beta_c \dot{\beta}_c \end{bmatrix} = \begin{bmatrix} \omega_v \cos\beta_c - \omega_o \sin\beta_c \cos\phi_c \\ -\omega_r \cos\beta_c - \omega_o \sin\beta_c \sin\phi_c \\ \omega_r \sin\beta_c \cos\phi_c + \omega_v \sin\beta_c \sin\phi_c \end{bmatrix} \tag{28}$$

and re-arranged to give

$$
\begin{bmatrix}
0 & \cos\beta_c & -\sin\beta_c\cos\phi_c \\
-\cos\beta_c & 0 & -\sin\beta_c\sin\phi_c \\
\sin\beta_c\cos\phi_c & \sin\beta_c\sin\phi_c & 0
\end{bmatrix}
\underbrace{}_{A}
\cdot
\begin{bmatrix}
\omega_r \\
\omega_v \\
\omega_o
\end{bmatrix}
=
\begin{bmatrix}
-\sin\beta_c\cos\phi_c\dot\phi_c - \cos\beta_c\sin\phi_c\dot\beta_c \\
-\sin\beta_c\sin\phi_c\dot\phi_c + \cos\beta_c\cos\phi_c\dot\beta_c \\
-\sin\beta_c\dot\beta_c
\end{bmatrix}
\tag{29}
$$

The A matrix is singular because its determinant is found to be zero. One of the velocity

components is linearly dependent on the other two and hence multiple solutions for $^L\vec\omega_B$ exist.

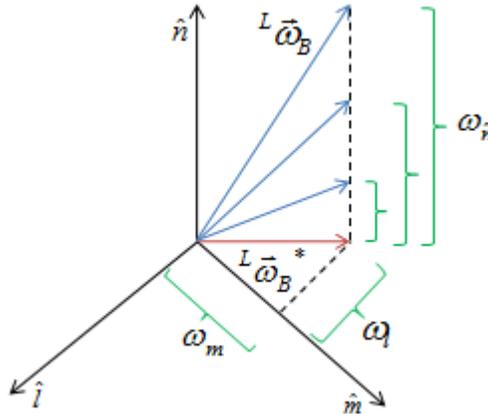Figure 18 depicts the meaning of multiple solutions in this case.

Figure 18: Multiple Angular Velocity Solutions

In Figure 18, $^L\vec\omega_B$ is expressed in the B-frame components. All solutions have the same $\hat{l}$ and $\hat{m}$

components but different $\hat{n}$ components because the use of $^L\vec\omega_B \times \hat{n}_c$ equation makes the $\hat{n}$ velocity

component arbitrary (the kinematic equation 27 can only describe two velocity components

uniquely). However, the B-frame is defined to have no component of the angular velocity in the

$\hat{n}$ direction. This requires the $\hat{n}$ velocity component to be zero. Thus, the unique angular velocity

solution, $^L\vec\omega_B{}^*$ can be obtained by projecting one of the $^L\vec\omega_B$ solutions onto the plane defined by $\hat{n}_c$

such that no component of the angular velocity occurs in the sail normal direction.

$$
{}^L\vec\omega_B{}^* = \left(I_{3x3} - \hat{n}_c\cdot\hat{n}_c\right){}^L\vec\omega_B = {}^L\vec\omega_B - \left(\hat{n}_c\cdot{}^L\vec\omega_B\right)\hat{n}_c
\tag{30}
$$

The unique solution is obtained by removing any velocity component in the $\hat{n}_c$ direction. Now, the simulation and desired angular momentum vectors can be expressed as

$$\vec{h}_S = I_n(\omega_1) \cdot \hat{n} + I_T(\omega_2) \cdot \hat{l} + I_T(\omega_3) \cdot \hat{m} \tag{31}$$

$$\vec{h}_c = I_n(\omega_{nc}) \cdot \hat{n}_c + I_T \cdot \left(\omega_o \cdot (I_{3x3} - \hat{n}_c \cdot \hat{n}_c) \cdot \hat{o} + {}^L\vec{\omega}_B^* \right) \tag{32}$$

where ω_1, ω_2 and ω_3 are the B-frame components of ${}^A\vec{\omega}_C$, and ω_{nc} is the desired inertial sail spin given by

$$\omega_{nc} = \begin{cases} zero\_spin \rightarrow \hat{n}_c \cdot {}^A\vec{\omega}_C = \hat{n}_c \cdot \left({}^A\vec{\omega}_L + {}^L\vec{\omega}_B^* + {}^B\vec{\omega}_C \right) = \hat{n}_c \cdot {}^A\vec{\omega}_L = \hat{n}_c \cdot \omega_o \hat{o} \\ equilibrium\_spin \rightarrow \hat{n}_c \cdot \left({}^A\vec{\omega}_L + {}^L\vec{\omega}_B^* + {}^B\vec{\omega}_C \right) = \hat{n}_c \cdot \left({}^A\vec{\omega}_L + {}^B\vec{\omega}_C \right) = \hat{n}_c \cdot \omega_o \hat{o} + \hat{n}_c \cdot \omega_s \hat{n}_c \end{cases} \tag{33}$$

because $\hat{n}_c \cdot {}^L\vec{\omega}_B^* = 0$ and choosing ${}^B\vec{\omega}_C = 0$ for no sail spin rate relative to the L-frame for the zero sail spin case. The angular momentum error is then found to be

$$\Delta {}^A\vec{h}_C = \vec{h}_S - \vec{h}_c$$

$$\Delta {}^A\vec{h}_C = \underbrace{I_n \omega_1 \hat{n} - I_n \omega_{nc} \hat{n}_c + I_T \cdot \omega_o \cdot \left((I_{3x3} - \hat{n} \cdot \hat{n}) \cdot \hat{o} - (I_{3x3} - \hat{n}_c \cdot \hat{n}_c) \cdot \hat{o} \right)}_{\Delta n\_term} + \underbrace{\left[I_T \cdot \left({}^L\vec{\omega}_B - {}^L\vec{\omega}_B^* \right) \right]}_{\Delta\omega\_term} \tag{34}$$

where the error term is decomposed into and expressed as a function of sail normal angular position and sail normal angular velocity components. In order to determine a control torque $\tau_{control}$ that reduces the angular momentum error, a Lyapunov stability approach will be used. First, a Lyapunov function candidate is defined.

$$V = \frac{1}{2} \left(\vec{h}_S - \vec{h}_c \right)^T \left(\vec{h}_S - \vec{h}_c \right) \tag{35}$$

From equation 35, the function V is positive definite with respect to angular momentum error. The behavior of the derivative of V can then be used to infer the behavior of the angular momentum error.

$$\frac{dV}{dt} = \frac{{}^L d\left(\vec{h}_S - \vec{h}_c\right)^T}{dt} \cdot \left(\vec{h}_S - \vec{h}_c\right) = \left[\frac{{}^A d\left(\vec{h}_S - \vec{h}_c\right)^T}{dt} - {}^A \omega_L \times \left(\vec{h}_S - \vec{h}_c\right)\right] \cdot \left(\vec{h}_S - \vec{h}_c\right)$$
$$= \frac{{}^A d\left(\vec{h}_S - \vec{h}_c\right)^T}{dt} \cdot \left(\vec{h}_S - \vec{h}_c\right) \tag{36}$$

Because the inertial derivative of angular momentum yields torque, the derivative of V can also

be expressed as

$$\frac{dV}{dt} = \left(\tau_S - \tau_c\right)^T \cdot \left(\vec{h}_S - \vec{h}_c\right)$$
$$\tau_S = \tau_{Se} + \tau_{control} \tag{37}$$
$$\tau_c = \tau_{ce} + \tau_{stay\_cone}$$

where τ_S and τ_c are total torques of the actual (simulation) and desired coning trajectory, τ_{Se} and

τ_{ce} are environmental torques of the simulation and coning trajectory, τ_{stay_cone} and $\tau_{control}$ are the

additional torques required to stay on the desired cone and the control torque applied in the

simulation, respectively. The derivative of V becomes

$$\frac{dV}{dt} = \left(\tau_{control} - \tau_{stay\_cone} + \delta\tau_e\right)^T \cdot \left(\vec{h}_S - \vec{h}_C\right)$$
$$\delta\tau_e = \tau_{Se} - \tau_{ce} \tag{38}$$

In order to ensure that the derivative of V remains negative definite with respect to the angular

momentum, $\tau_{control}$ should be chosen as

$$\tau_{control} = -k_{control} \cdot \left(\vec{h}_S - \vec{h}_C\right) + \tau_{stay\_cone} - \delta\tau_e \tag{39}$$

which enables the derivative of V to be negative definite, as desired.

$$\frac{dV}{dt} = -k_{control}\left(\vec{h}_S - \vec{h}_C\right)^T \cdot \left(\vec{h}_S - \vec{h}_C\right) \tag{40}$$

The stability analysis proves that $\Delta {}^A\vec{h}_C$ decays to zero [26] and thus the control law enables $\vec{h}_S$ to

track $\vec{h}_c$, for any positive control gain, $k_{control}$.

This seems to be a nice result. Unfortunately, from examining the decomposed components within the angular momentum error (equation 34), the Lyapunov function is not positive definite with respect to the sail normal because V can be zero even when sail normal is not (a combination of non-zero sail normal angular position error and velocity error can enable V to become zero). Thus, whether the sail normal error ($\Delta\hat{n} = \hat{n} - \hat{n}_c$) decays to zero has not been proven. Since the angular momentum error is a function of sail normal angular position (equation 34), the control law reducing $\Delta^A\vec{h}_C$ is implemented anyway (below) with the hope that $\Delta^A\vec{h}_C \to 0$ can cause $\Delta\hat{n} \to 0$ and enable $\hat{n}$ to track the desired $\hat{n}_c$ on the coning trajectory.

The environmental torques act on the sail based on its attitude, and these attitudes differ in the simulation and on the desired coning trajectory, unless the simulation trajectory exactly matches the desired coning motion. Since the application of control torque $\tau_{control}$ is intended to enable $\Delta\vec{h} \to 0$, and that may cause simulation sail attitude, $\hat{n} \to$ desired cone sail attitude, $\hat{n}_c$, it may be reasonable to assume that $\delta\tau_e$ is small. In this case

$$\frac{dV}{dt} = \left(\tau_{control} - \tau_{stay\_cone}\right)^T \cdot \left(\vec{h}_S - \vec{h}_C\right)$$

$$\tau_{control} = -k_{control} \cdot \left(\vec{h}_S - \vec{h}_C\right) + \tau_{stay\_cone} \tag{41}$$

The τ_{stay_cone} can be given by

$$\tau_{stay\_cone} = \tau_c - \tau_{ce} \tag{42}$$

where τ_c is the torque required to trace the desired cone, which is rather complicated to calculate on-line (inertial derivative of the desired angular momentum, equation 32). The environmental torques on the desired cone, τ_{ce} involve many estimates of environmental factors and thus their analytical predictions can become inaccurate. If possible, such calculations (variables involving

many unknowns) on a small sailcraft should be avoided. They can be avoided with the idea that

in $\tau_{control}$, $k_{control}$ is a user-defined constant term and can be chosen large enough such that its term

in equation 41 dominates the effect of τ_{stay_cone}. With these simplifications, the Lyapunov

function and control torque are approximated by

$$\frac{dV}{dt} = \left(\tau_{control}\right)^T \cdot \left(\vec{h}_S - \vec{h}_C\right)$$
$$\tau_{control} = -k_{control}\left(\vec{h}_S - \vec{h}_C\right)$$

(43)

The next section examines the behavior of this simplified control law.

III.2. *Angular Momentum Error Reduction Results and Discussion*

The sail dynamics under the influence of environmental torques are presented for the zero

and equilibrium sail spin rates. For the zero sail spin, the results for the equilibrium points,

$[\beta = 35°, \phi = 0°]$ - orbit lowering and $[\beta = 145°, \phi = 180°]$ - orbit raising are given. These two

equilibrium points were selected because they induced the largest orbital effects (energy, angular

momentum and eccentricity) for 1° cones (see Appendix A). The robustness of the control

method is tested by adding initial condition errors to the sail angular position (these simulate

errors in the sail attitude that emerge from disturbances) and using larger coning cones (greater

orbital effects can be induced with cones larger than 1°).

III.2.1. *Orbit Lowering Case with Zero Sail Spin*

In the orbit lowering case, the thrust is in the anti-velocity direction. The equilibrium

point used is $\beta = 35°, \phi = 0°$. The control method performance in tracing the desired cone at orbit

rate is examined. The control method is designed to reduce the angular momentum error. The

Lyapunov function indicates the performance of the control method for reducing this error.
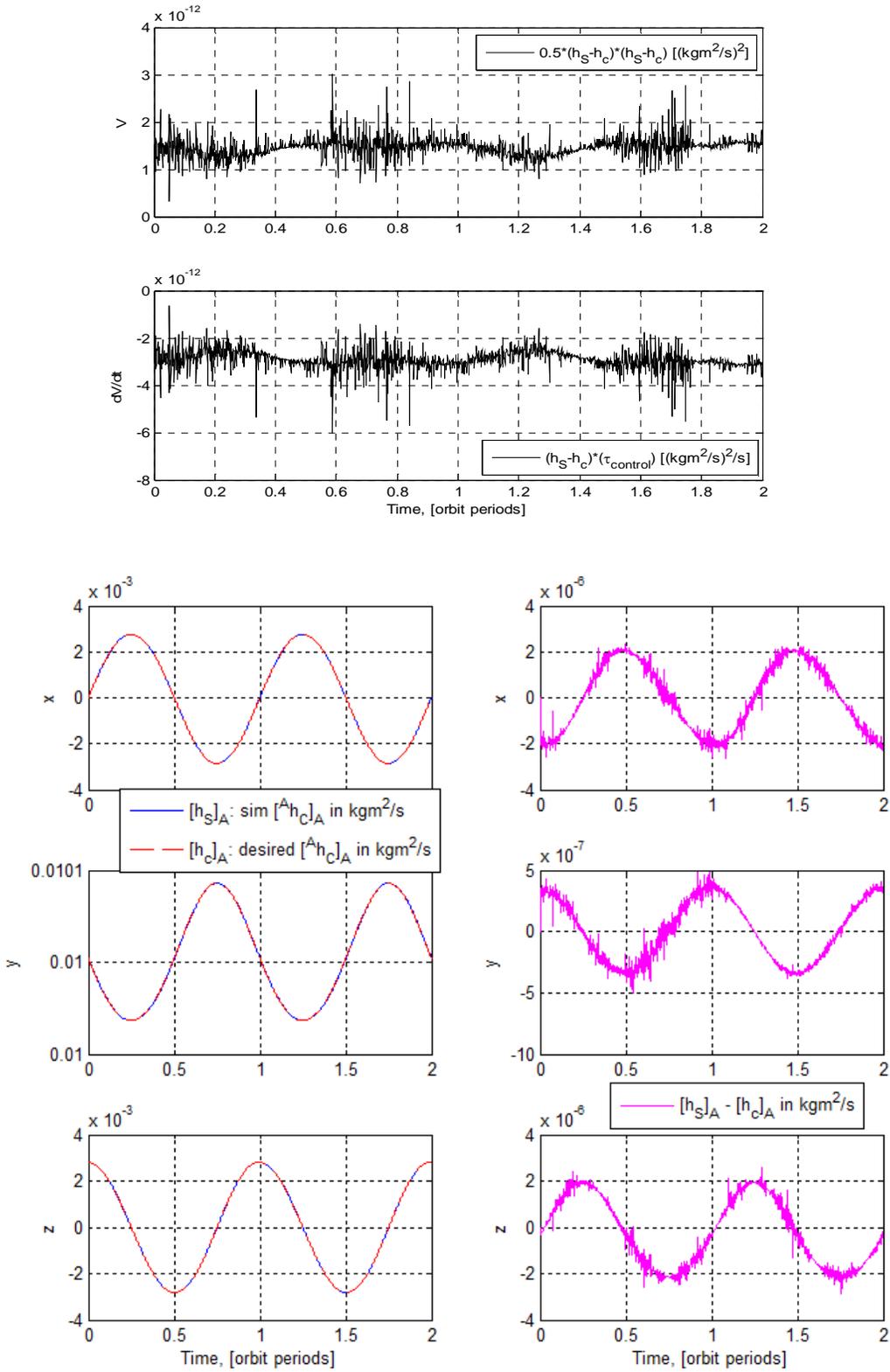
Figure 19: Lyapunov Function, Its Approximated Derivative and A-frame Angular Momentum Components for Coning Trajectory having Half Cone Angle, $\delta=1°$ about a Nominal Sail Normal of $\beta_0=35°$, $\Phi_0=0°$

The Lyapunov function V in Figure 18, and thus the angular momentum error magnitude, is significantly lower than the absolute sailcraft angular momentum ($\sim 10^3$ times lower). This indicates that the control method is successful in reducing the angular momentum error. On the other hand, even though the (approximate) derivative of V is always negative, the function V does not monotonically decrease. The derivative of V was approximated from

$$\frac{dV}{dt} = \left(\tau_{control} - \tau_{stay\_cone} + \delta\tau_e \right)^T \cdot \left(\vec{h}_S - \vec{h}_C \right) \text{ to } \frac{dV}{dt} = \left(\tau_{control} \right)^T \cdot \left(\vec{h}_S - \vec{h}_C \right) \text{ with simplifying}$$

assumptions eliminating τ_{stay_cone} and $\delta\tau_e$, as discussed earlier. In order to understand the incompatible behavior between V and its approximated derivative, the individual torque components in the non-approximated derivative are examined in Figure 20.
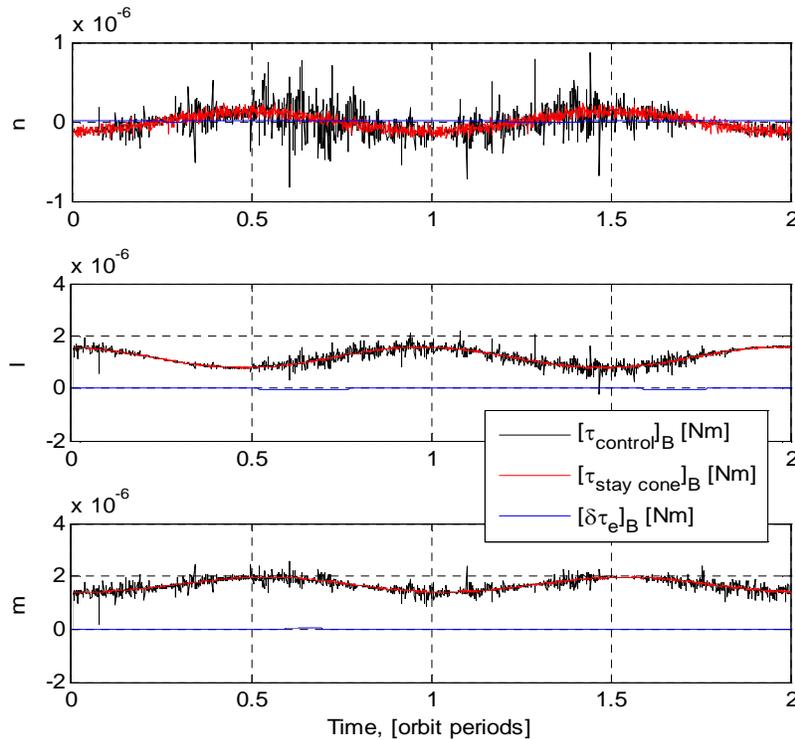

Figure 20: Torques of the System in the B-frame

The $\tau_{control}$ is approximated using $-k_{control}\left(\vec{h}_S - \vec{h}_C\right)$. The magnitude is on the order of 10^{-6} Nm, which is reasonably sized for a small sailcraft. For a similar 3 kg and 40 m^2 solar sail, magnetic control was used to enable inertial coning of the sail normal at orbit rate and predicted maximum control torques on the order of 10^{-5} Nm [8]. In Figure 20, the $\delta\tau_e$ torque is ~10^3 times lower in magnitude than $\tau_{control}$ and τ_{stay_cone}, justifying the assumption of elimination $\delta\tau_e$ from equation 41 ($\delta\tau_e$ is negligible as compared with $\tau_{control}$ and τ_{stay_cone}). Note, however, that the τ_{stay_cone} torque is nearly identical (except for numerical noise) to the $\tau_{control}$. The τ_{stay_cone} is determined numerically by calculating the total torque τ_c required for precessing the angular momentum on the desired cone and deducting the environmental torques, τ_{ce} from τ_c (equations 42 and 44). The total torque on the desired cone, τ_c is the inertial derivative of the desired angular momentum, $\dot{\vec{h}}_c$. A numerical solution for τ_c can be obtained via a finite difference

$$\tau_c = \frac{\vec{h}_{c2} - \vec{h}_{c1}}{t_2 - t_1} = \frac{\Delta\vec{h}_c}{\Delta t} \tag{44}$$

where $\Delta\vec{h}_c$ is the change in desired angular momentum over a period of time, Δt. The $\vec{h}_{c1}$ and $\vec{h}_{c2}$ are calculated at times t and $t + \Delta t$ via equation 32. The magnitude of Δt is decreased enough (with machine limitations) to approximate $\Delta t \rightarrow 0$. When the non-approximated derivative of V is used that includes the effects of τ_{stay_cone} and τ_{ce}, the Lyapunov function and its derivative correspond to each other.
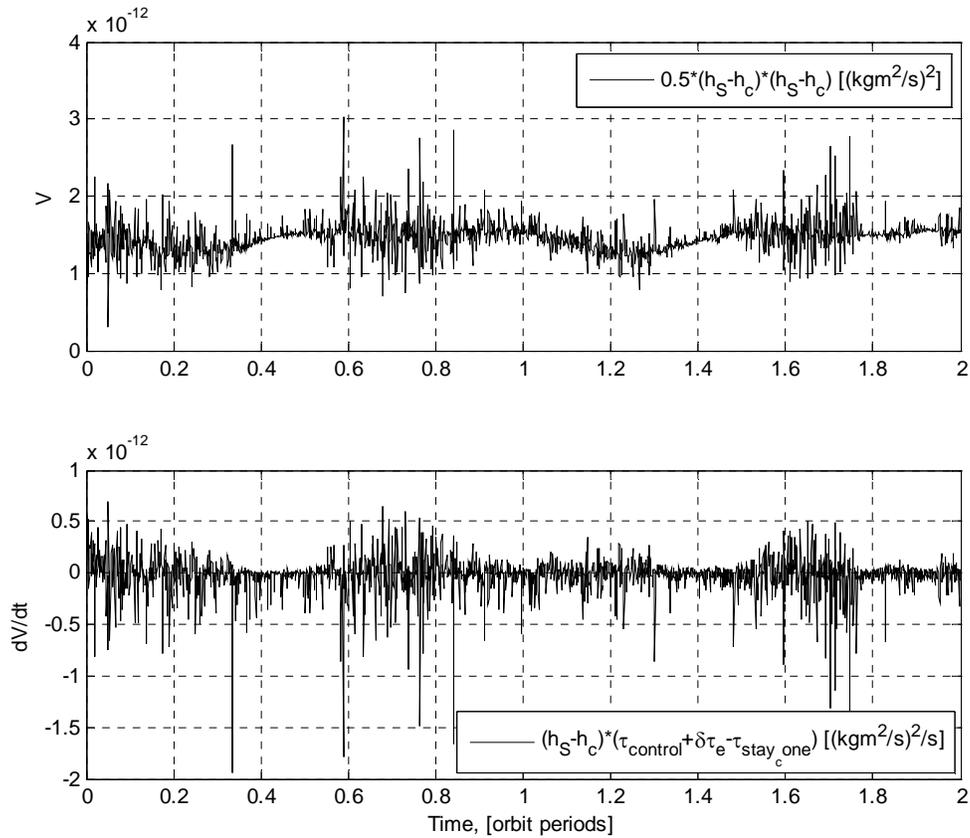
Figure 21: Lyapunov Function and Its Derivative

The derivative is no longer always negative explaining why *V* does not decrease. Even though *V*

does not decrease, the oscillations of *V* are bounded. This indicates that the momentum errors

within the system remain bounded and do not grow with time. Since *V* is a measure of the

angular momentum error, the control method thus enables the sail angular momentum to trace

the desired with some small, bounded error. The acceptable nature of this error in the cone

tracing is discussed later in this section.

One may wonder why, in Figure 20, the τ_{stay_cone} torque is essentially identical to the

control torque, $\tau_{control}$. Observe that the actual torque on the system from the simulation, τ_S and

total torque required to stay on the desired cone, τ_c are given by

$$\tau_S = \tau_{actual/sim} = \tau_{se} + \tau_{control}$$
$$\tau_c = \tau_{required} = \tau_{ce} + \tau_{stay\_cone} \tag{45}$$

When $\delta\tau_e$ is negligible, the environmental torques τ_{se} and τ_{ce} can be expressed as

$$\delta\tau_e = \tau_{Se} - \tau_{ce} \to 0 \Rightarrow \tau_{Se} = \tau_{ce} = \tau_e \tag{46}$$

from which the total system and desired cone torques become

$$\tau_S = \tau_{actual/sim} = \tau_e + \tau_{control}$$
$$\tau_c = \tau_{required} = \tau_e + \tau_{stay\_cone} \tag{47}$$

From these equations, in order to trace the desired cone and induce the required angular

momentum precession rate, we *must* have the total simulation torque, $\tau_S \to$ the desired cone

torque, τ_c. This explains the behavior in Figure 20, where $\tau_{control}$ is found to be identical to

τ_{stay_cone}.

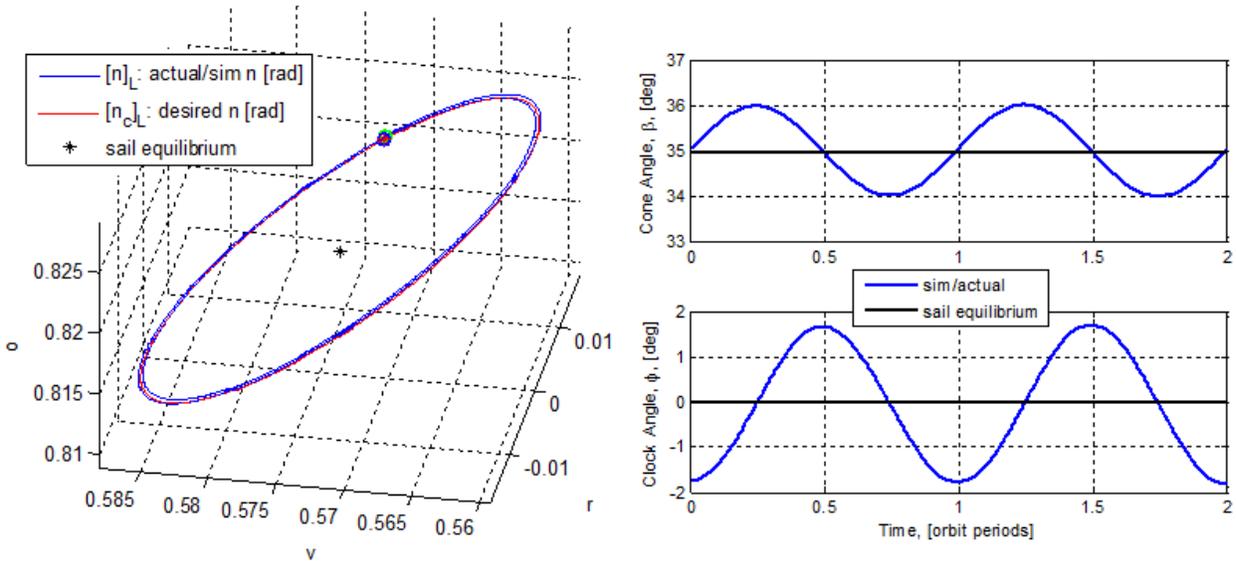The corresponding behavior for the sail normal is shown in Figure 22.

Figure 22: Sail Angular Positions for Coning Trajectory having Half Cone Angle, δ=1° about a
Nominal Sail Normal of β₀=35°, Φ₀=0° in the L-frame

The three-dimensional plot indicates that the control method enables the simulation sail normal

$\hat{n}$ to trace the desired circular cone. The simulation and desired trajectories in this case begin at

the same initial conditions. In the cone and clock angles plot, both β and ϕ complete one cycle in

one orbital period and repeat the same pattern in the next orbital period. Thus, the control method

also enables orbit rate coning. The errors in the individual components of sail normal in the
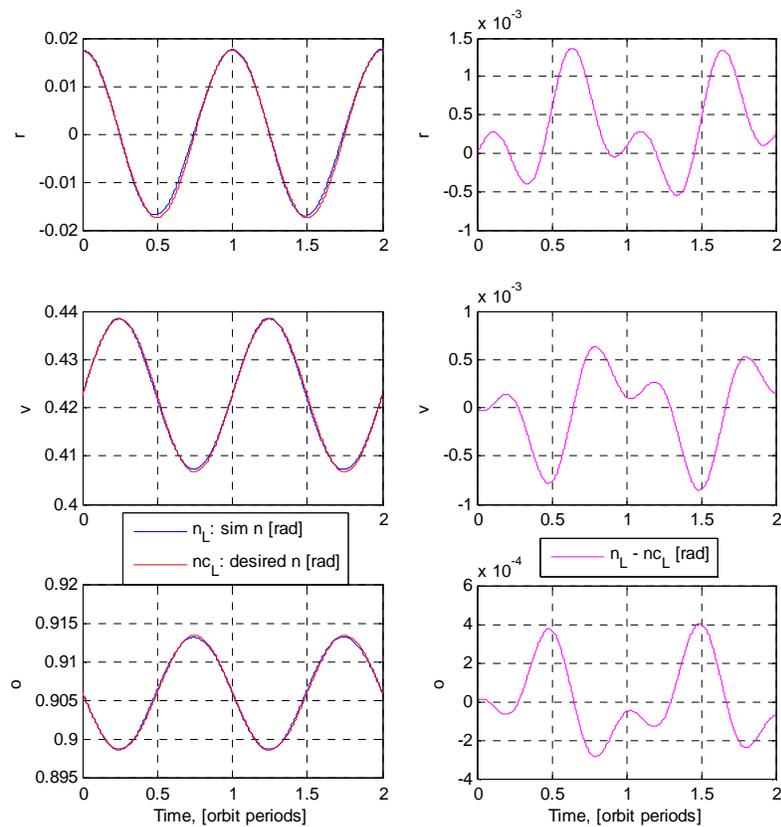
coning tracing are shown in Figure 23.

Figure 23: Individual L-frame Components of Simulated and Desired Sail Normal with Errors

As the cone is traced, Figure 23 shows that the error magnitudes of the $\hat{r}$, $\hat{v}$ and $\hat{o}$ sail normal

components oscillate. Even though there are errors in the coning tracing, they appear to be

bounded. In addition, the error magnitudes are significantly lower than the absolute component

magnitudes (10^1-10^3 times lower). McMahon, et. al. assert that the shape of the coning need not

be accurate as long as orbit rate coning is achieved in order to yield the orbital effects [13]. Thus, slight deviations from the circular coning are not expected to have significant deviations in the averaged orbital effects induced over an entire orbit.

A sensitivity analysis is performed where the control gain, $k_{control}$ is varied to study the maximum angular position error between the simulated and desired sail normal. The angular position error definition is illustrated in Figure 24.
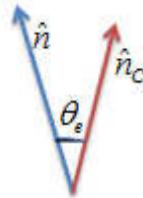

Figure 24: Angular Position Error

The angular difference between the desired and simulated sail normal is defined as the angular position error. The $k_{control}$ was varied over a range of 0-2 and the variation in maximum angular error (over one orbital period) was studied. In order to understand the results, the angular error between the simulated and desired angular momentum is also shown.
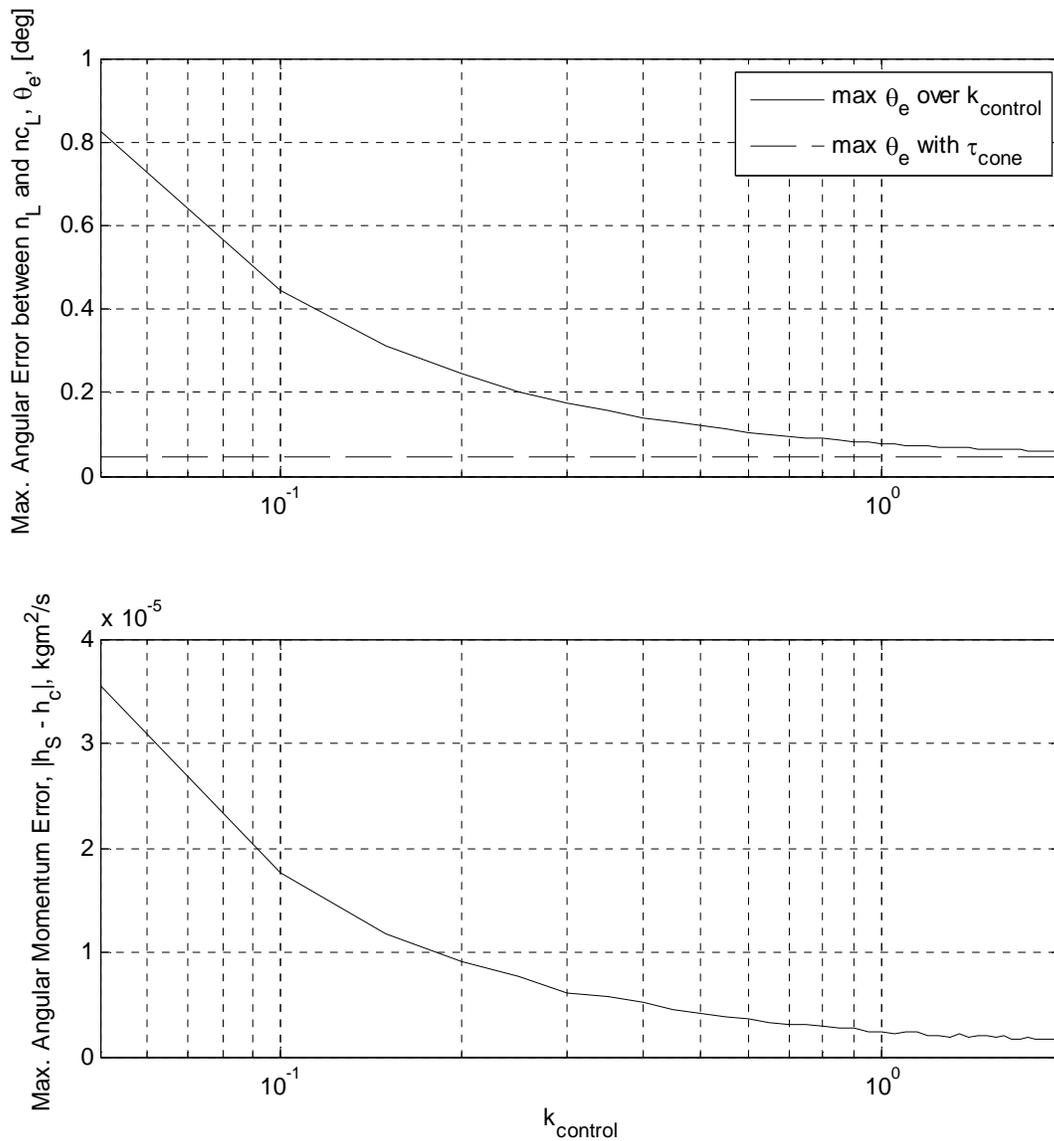
Figure 25: Sensitivity Analysis of Maximum Angular Position and Momentum Error (for One Orbital Period) to variations in $k_{control}$

The angular position error, θ_e decreases more rapidly with steadily increasing $k_{control}$. As the

magnitude of $k_{control}$ increases, the decrease in θ_e becomes less rapid, until the limiting θ_e of 0.05° is

reached (indicated by the dashed line). Smaller $k_{control}$ magnitudes result in smaller control torque

magnitudes at each time step. With smaller control torque magnitudes, the simulated angular

momentum is not corrected to trace the desired angular momentum as rapidly. This means that

the angular momentum error is larger for smaller $k_{control}$ magnitudes. As $k_{control}$ increases, the angular momentum is corrected more rapidly to trace the desired. This results in a smaller error. The angular momentum error decays rapidly with increasing $k_{control}$. Since the angular position error is a function of angular momentum error, the θ_e also decays in a similar fashion. Ideally, the error should decay to zero as increasing control torque will enable the simulation to trace the desired exactly. However, the θ_e decays to a limiting value and not zero. This is because θ_e is calculated using the simulated trajectory and desired *analytical* trajectory, whereas the control torque is a function of simulated trajectory and desired *numerical* trajectory. This means that the simulated trajectory traces the desired *numerical* trajectory and not *analytical*. The difference between *analytical* and *numerical* desired trajectories is shown in Figure 26.
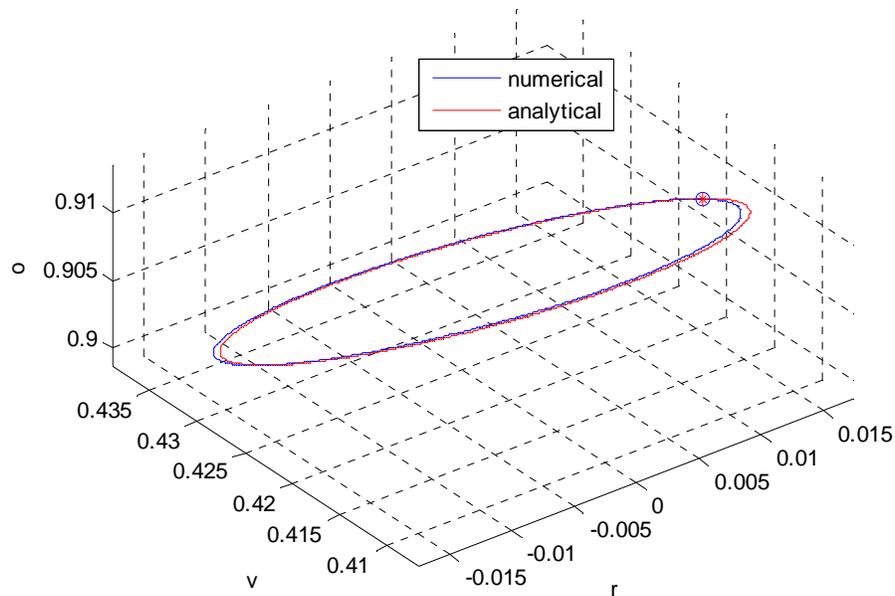

Figure 26: Numerical and Analytical Desired Coning Trajectories having Half Cone Angle, δ=1° about a Nominal Sail Normal of β₀=35°, Φ₀=0° (One Orbital Period)

The total torque on a coning trajectory (half cone angle, $\delta = 1°$) for a given nominal $\beta_0 = 35°$ and $\phi_0 = 0°$ is calculated using equation 44 (calculate τ_c). This torque was applied in the simulation to yield the *numerical* coning trajectory. Differences exist because the instantaneous derivative of desired angular momentum is not available (τ_c is calculated numerically). The maximum angular position error between the *analytical* and *numerical* coning trajectories was found to be 0.05°. Hence, the θ_e in Figure 25 decays to the numerical desired trajectory and reaches a limiting value of 0.05° (same as the maximum angular position error between the *analytical* and *numerical* coning trajectories).

The performance of the control method with the exact initial conditions has been presented so far. Practically, internal/external disturbances on the sailcraft causes initial condition errors with the sail attitude. Thus, the performance with initial condition errors should also be analyzed. Figure 27 illustrates how initial condition errors are added to the system.
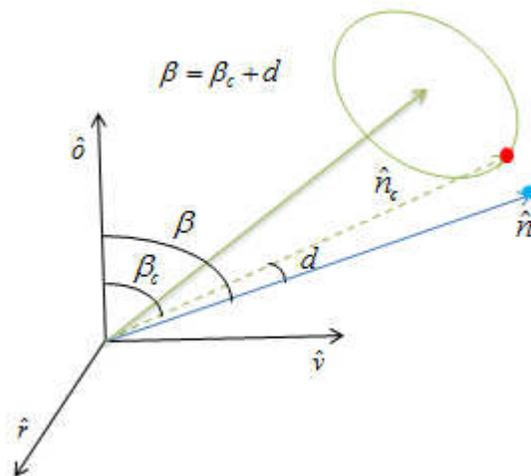

Figure 27: Initial Condition Error

The red dot represents the exact initial conditions for the system. The initial condition error is obtained by adding an angular deviation d such that the initial angular position (and hence initial

angular velocity) contains errors with respect to the desired coning trajectory. The control method performance for 1° and 10° deviations follows.
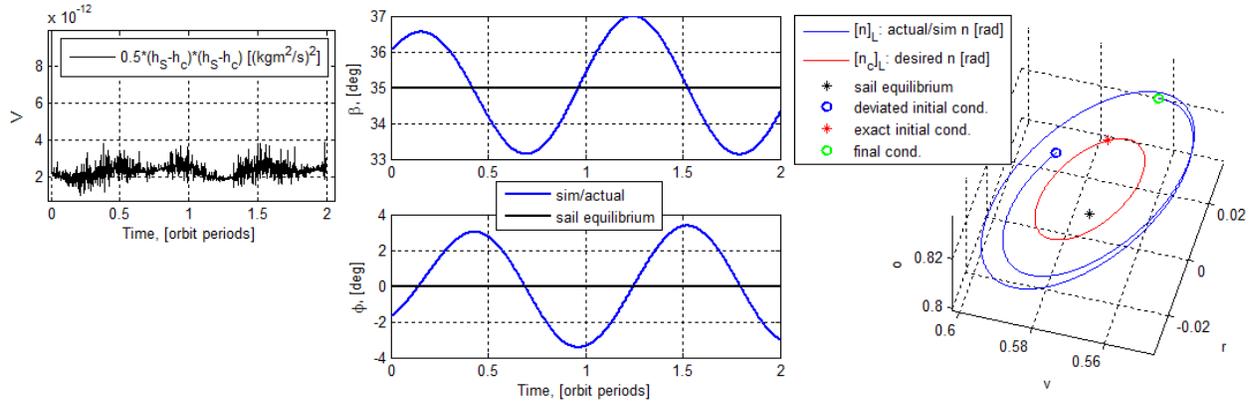

Figure 28: Control Method Performance in Tracking Desired Angular Momentum and Sail Normal with Initial Condition Error of 1° (d=1°), Zero Sail Spin

The Lyapunov function decreases to the levels as with no initial condition errors. This means that the control method is able to track the desired angular momentum vector even with the initial condition error. The sail normal motion is coning about the sail equilibrium point, however the desired normal is not traced as well as with no initial condition errors. The rate of coning has also deviated slightly from orbit rate. The Lyapunov function levels drop to the expected levels after one time step. This is clearly evident in the sail angular momentum vector motion shown in Figure 29.
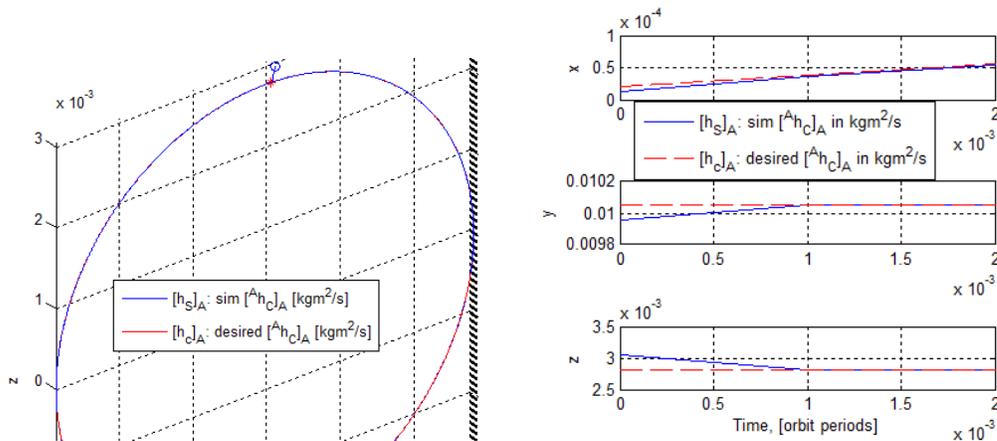

Figure 29: Simulated and Desired Angular Momentum for Coning Trajectory with Initial Condition Error, d=1°, $k_{control}=1$

As expected, as the control authority is decreased $\left(k_{control} = 0.1\right)$, the simulation angular

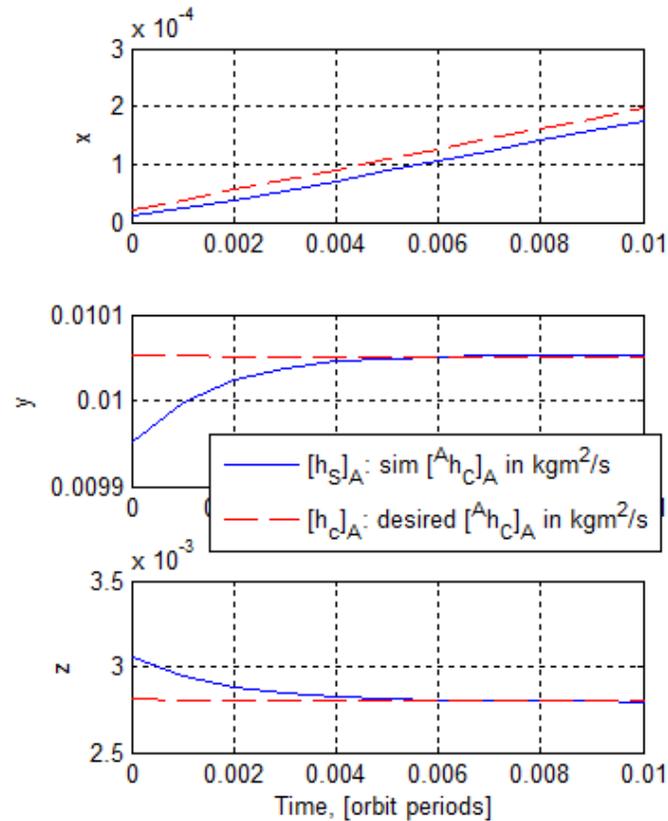momentum tracks the desired cone more gradually (see Figure 30).

Figure 30: Simulated and Desired Angular Momentum for Coning Trajectory with Initial Condition Error, d=1°, k$_{control}$=0.1

With decreased control authority, the control torque application is reduced which enables the sail

angular momentum to track the desired gradually instead of after one time step. This behavior is

preferable in a small sailcraft to avoid any abrupt changes to the attitude that can damage the sail.

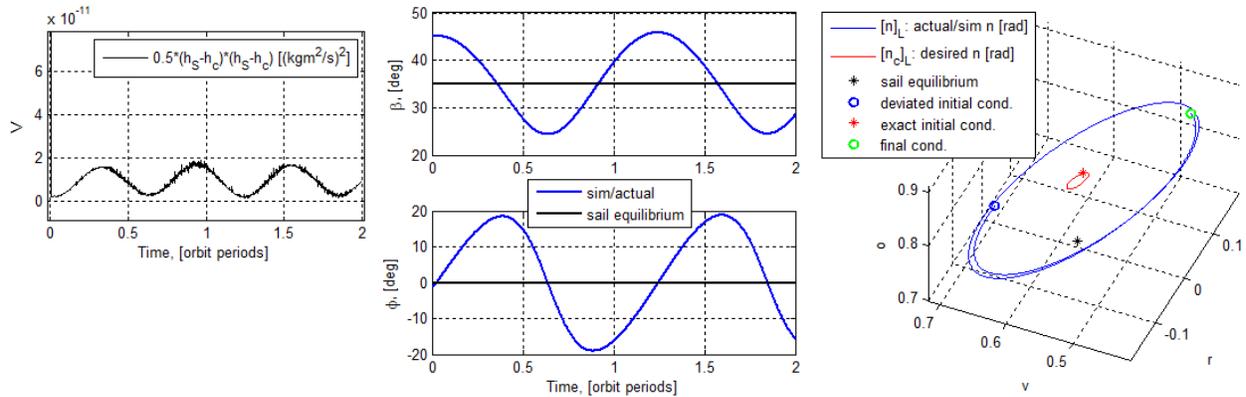The result with a larger initial condition error of 10° is presented in Figure 31.

Figure 31: Control Method Performance in Tracking Desired Angular Momentum and Sail Normal with Initial Condition Error of 10° (d=10°), Zero Sail Spin

The control method performance in tracing the desired angular momentum has deteriorated slightly, which is indicated by the Lyapunov function magnitude increase as compared with the 1° deviation case (~10 times increase). However, there is significant deterioration in tracing the desired sail normal as compared with the 1° error case. The sail normal appears to trace a larger cone at a slightly different rate. This means that even though the control method performance did not deteriorate noticeably in tracing the desired angular momentum, the performance degraded significantly in tracing the desired sail normal.

The control method robustness is further examined by analyzing the results for tracing larger cones (larger half-cone angles). The results for 5° and 60° cones are presented below.
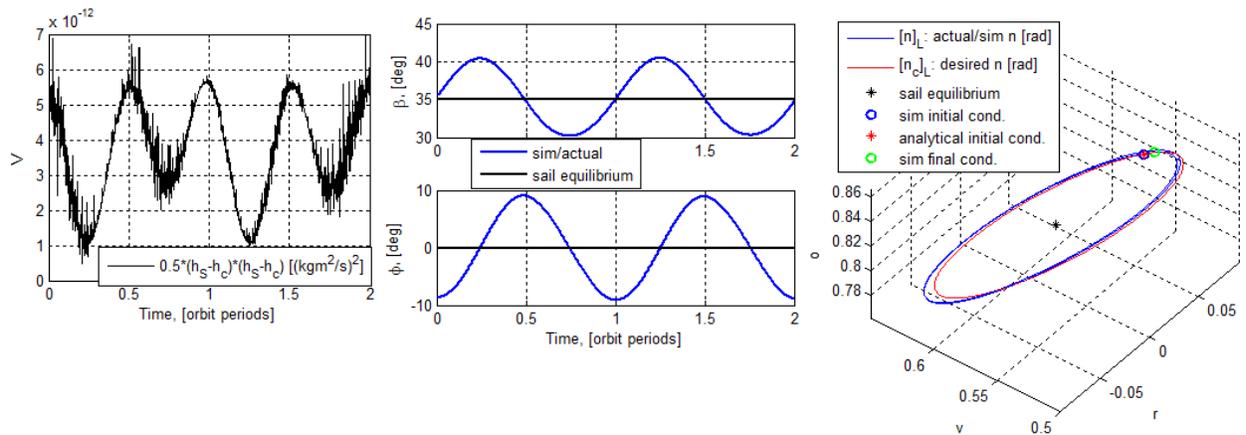

Figure 32: Control Method Performance in Tracking Desired Angular Momentum and Sail Normal with 5° cone, Zero Sail Spin

The errors from tracking the desired angular momentum are on the same order of magnitude as for the 1° cone (Lyapunov function level has the same order of magnitude). In addition, there are no significant deviations from orbit rate coning of the sail normal vector. The sail normal motion tracks the desired 5° circular cone with no significant differences as compared with the 1° cone case.
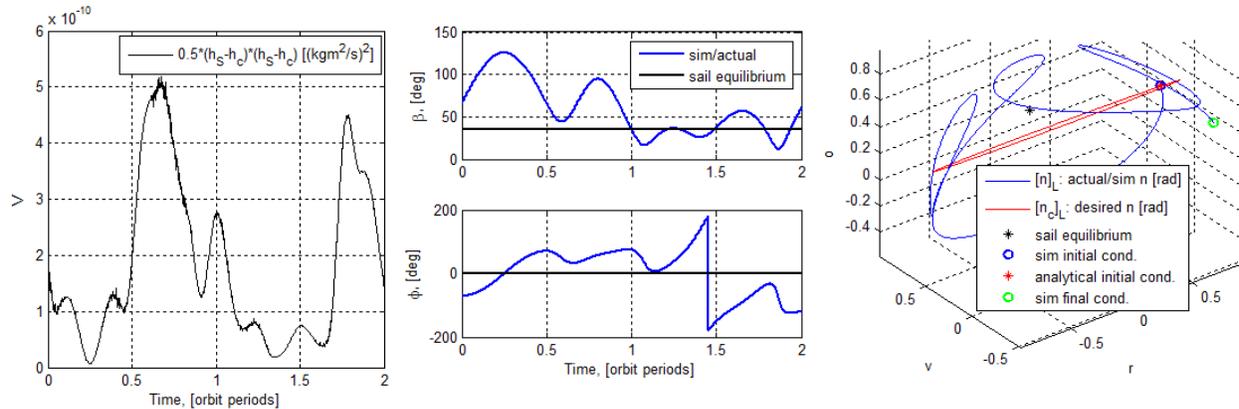

Figure 33: Control Method Performance in Tracking Desired Angular Momentum and Sail Normal with 60° cone, Zero Sail Spin

However, the control performance has deteriorated significantly for cones as large as 60°. The sail normal does not cone around the equilibrium point. The angular momentum tracking also has increased errors as compared with smaller cones ($\sim 10^2$ times larger).

III.2.2. *Orbit Raising Case with Zero Sail Spin*

In the orbit raising case, the thrust is applied in the velocity direction. The equilibrium point is $\beta = 145°, \phi = 180°$. The Lyapunov function behavior, *V* is presented in Figure 34.

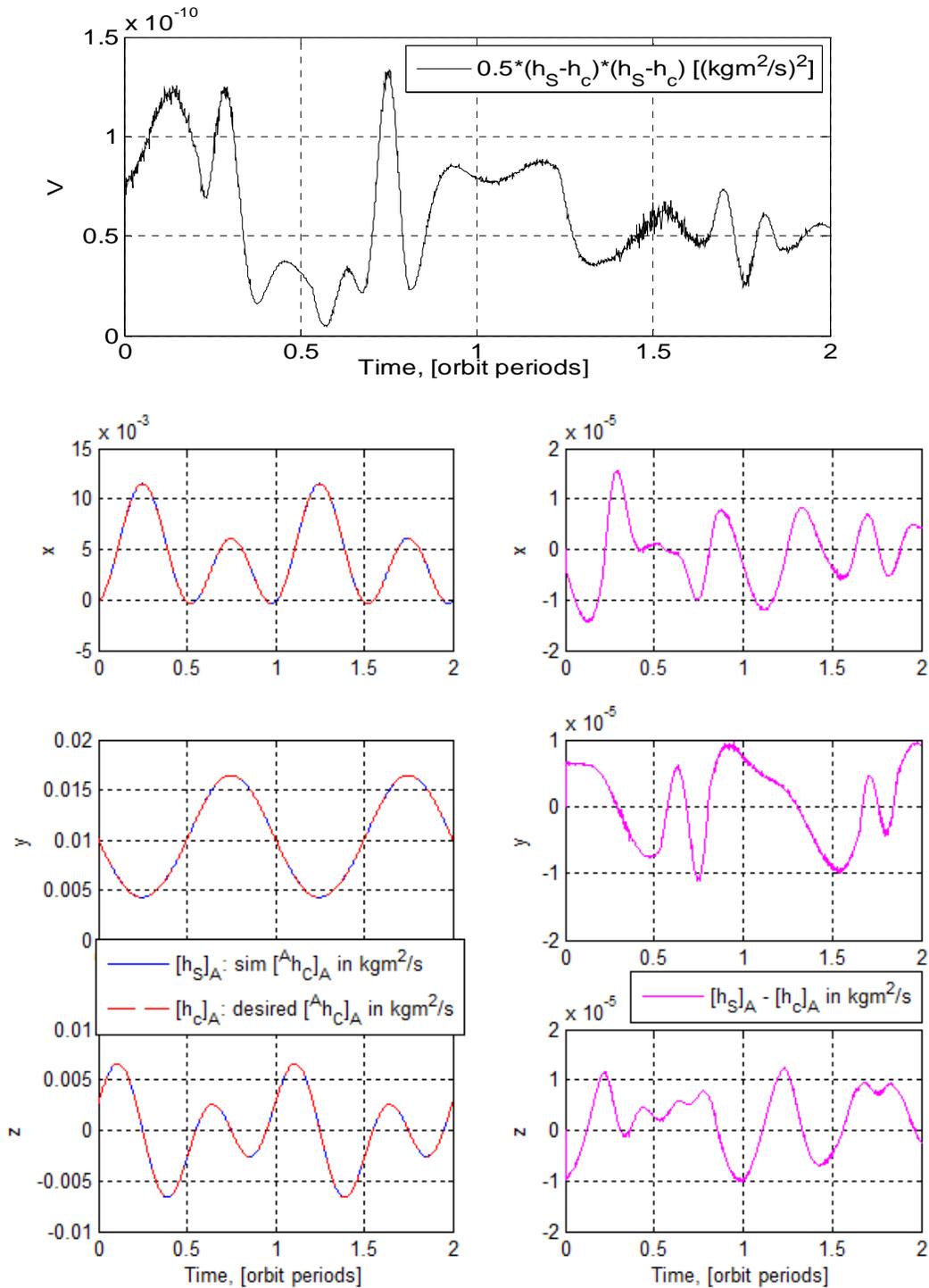Figure 34: Lyapunov Function, Its Approximated Derivative and A-frame Angular Momentum Components for Coning Trajectory having Half Cone Angle, $\delta=1°$ about a Nominal Sail Normal of $\beta_0=145°$, $\Phi_0=180°$

The Lyapunov function, V and thus the angular momentum error have small magnitudes as compared with the absolute sailcraft angular momentum ($\sim 10^2$-10^3 times lower). This indicates

that the control method is successful in reducing the angular momentum error. However, the control method does not enable the sail normal to trace the desired coning trajectory.
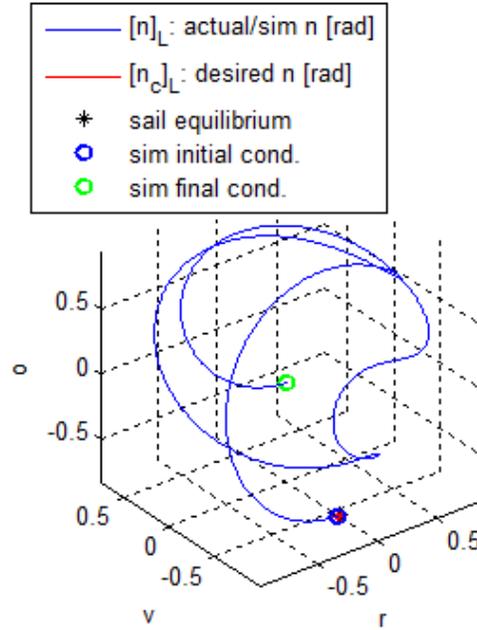

Figure 35: Sail Angular Positions for Coning Trajectory having Half Cone Angle, $\delta=1°$ about a Nominal Sail Normal of $\beta_0=35°$, $\Phi_0=0°$ in the L-frame

The red dot/circle represents the desired trajectory. Thus, the sail normal does not cone or even stay in the vicinity of the desired cone. Even though the angular momentum error is small and is able to trace the desired trajectory, the sail normal error does not. This can be explained by studying the behavior of individual terms in the angular momentum error.

$$\Delta^{A}\vec{h}_{C} = \underbrace{I_{n}\omega_{1}\hat{n} - I_{n}\omega_{nc}\hat{n}_{c} + I_{T} \cdot \omega_{o} \cdot \left((I_{3x3} - \hat{n} \cdot \hat{n}) \cdot \hat{o} - (I_{3x3} - \hat{n}_{c} \cdot \hat{n}_{c}) \cdot \hat{o}\right)}_{\Delta n\_term} + \underbrace{\left[I_{T} \cdot \left(^{L}\vec{\omega}_{B} - ^{L}\vec{\omega}_{B}^{\,*}\right)\right]}_{\Delta\omega\_term} \quad (48)$$

The following plot explains the behavior by examining the individual Δn_term and $\Delta\omega\_term$ that constitute the angular momentum error, $\Delta^{A}\vec{h}_{C}$.
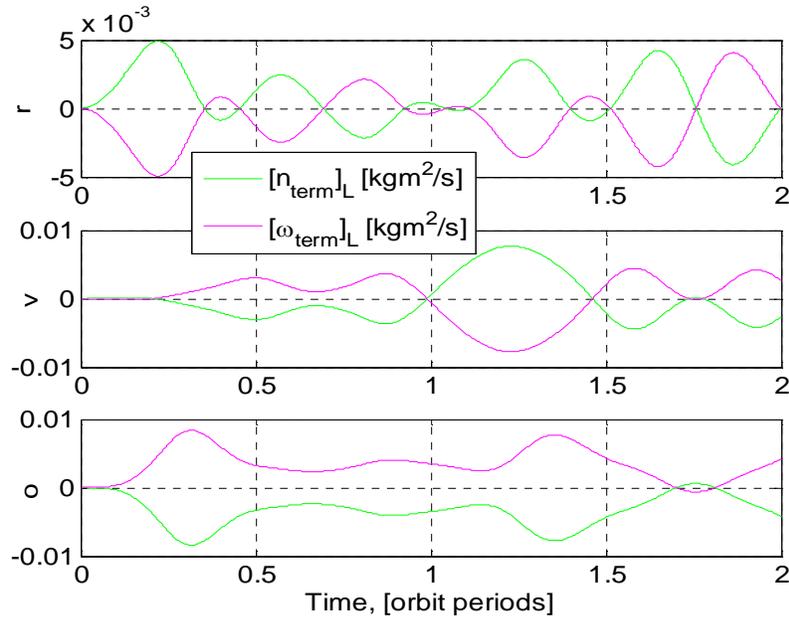
Figure 36: Individual Δn_{term} and $\Delta \omega_{term}$ terms (β_0=145°, Φ_0=180°)

The individual terms cancel each other, meaning that the combination of the terms tend to zero

even when the individual terms do not. As discussed in section III.1, the Lyapunov function is

positive definite with respect to the angular momentum, $\vec{h}$ and not with respect to the sail normal,

$\hat{n}$. Thus, $\Delta \vec{h} \rightarrow 0$ does not guarantee $\Delta \hat{n} = \hat{n} - \hat{n}_c \rightarrow 0$ and does not ensure that the sail normal

tracks the desired sail normal. In this simulation case, $\Delta \vec{h} \rightarrow 0$ indeed does not cause the

simulation sail attitude, $\hat{n} \rightarrow$ desired cone sail attitude, $\hat{n}_c$. Although the control method

performance for the angular momentum is as expected (traces the desired), the angular position

performance is not desirable.

III.2.3. Orbit Lowering Case with Equilibrium Sail Spin

In the orbit lowering case with zero sail spin, the sail normal was able to track the desired

trajectory at orbit rate as opposed to in the orbit raising case (could not track the desired coning

trajectory). Thus for comparison purposes, only the orbit lowering case for the equilibrium sail

spin is presented. The equilibrium sail spin rate was calculated to be -2.97×10^{-4} rad/s

($^B\vec{\omega}_C = \omega_s \cdot \hat{n}$ from equation 33). The Lyapunov function is given in Figure 37.
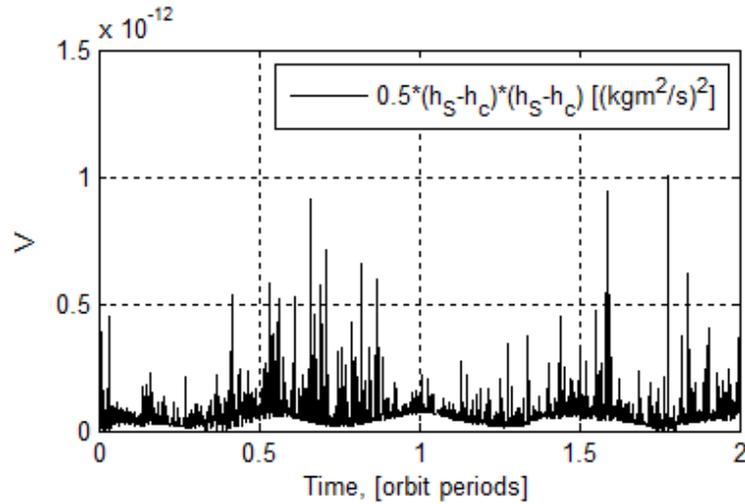
Figure 37: Lyapunov Function or Coning Trajectory having Half Cone Angle, $\delta=1°$ about a Nominal Sail Normal of $\beta_0=35°$, $\Phi_0=0°$

The Lyapunov function levels are on the same order of magnitude (10^{-12}), however the levels are

lower in magnitude (~2 times) as compared with the zero sail spin case (Figure 21). This

indicates that the control method performance is more effective in reducing the angular

momentum with the equilibrium spin. The cost at which this control performance is achieved is

given by the control torque.
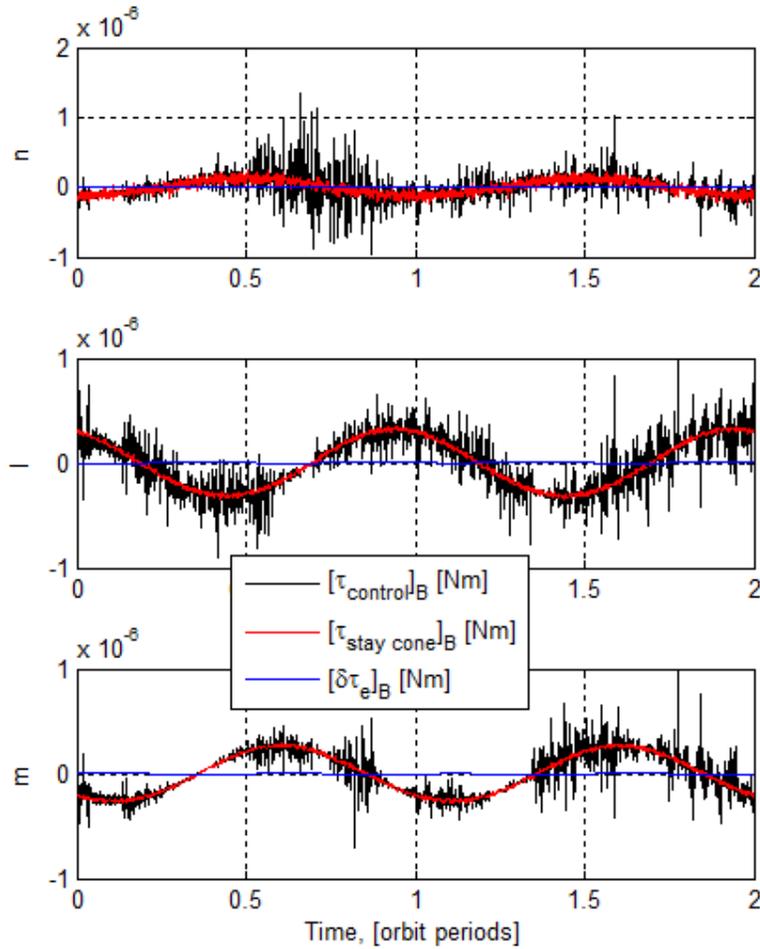
Figure 38: Torques of the System in the B-frame

Similar to the zero sail spin case (Figure 20), the magnitude of $\tau_{control}$ is on the order of 10^{-6} Nm

(reasonable to apply on small sailcraft) and the $\delta\tau_e$ torque is $\sim 10^3$ times lower in magnitude than

$\tau_{control}$ and τ_{stay_cone}, justifying the assumption of elimination $\delta\tau_e$ from equation 41 (see section

III.2.1 for more details). However, as compared with the zero sail spin case, the control torque

required in the $\hat{l}$ and $\hat{m}$ directions is lower in magnitude. Figure 39 shows a comparison between

the total control torque magnitude required in the equilibrium and zero sail spin cases.
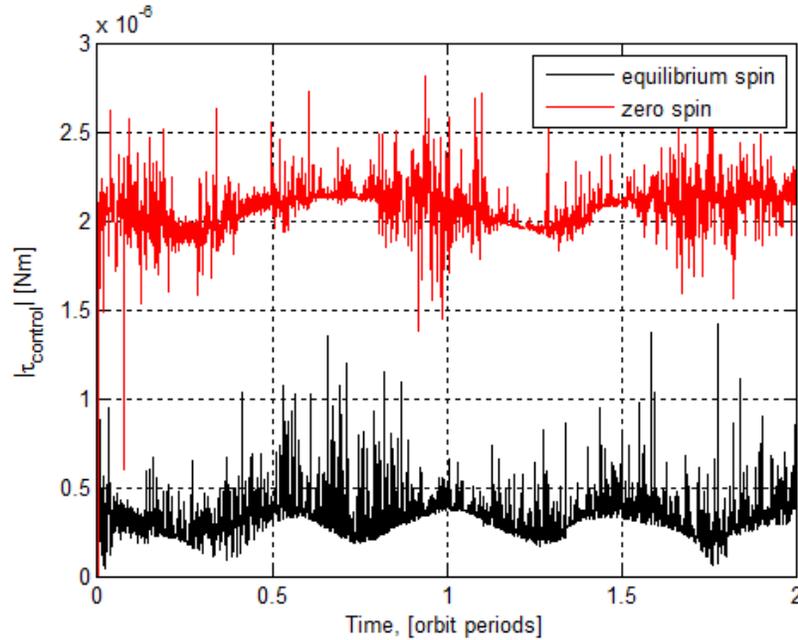
Figure 39: Control Torque Magnitude Required in the Equilibrium and Zero Sail Spin Rate Cases

The control torque, $\tau_{control}$ required to enable the desired orbit rate circular coning is less in magnitude in the equilibrium sail spin case than for the zero sail spin case (~4 times less). This indicates that the equilibrium spin case can provide better control method performance (angular momentum error magnitudes are lower as compared with those of the zero sail spin case - Figure 21 and Figure 37) with a smaller cost (due to the smaller control torque magnitudes).

The control method performance to enable sail normal tracing is shown in Figure 40.
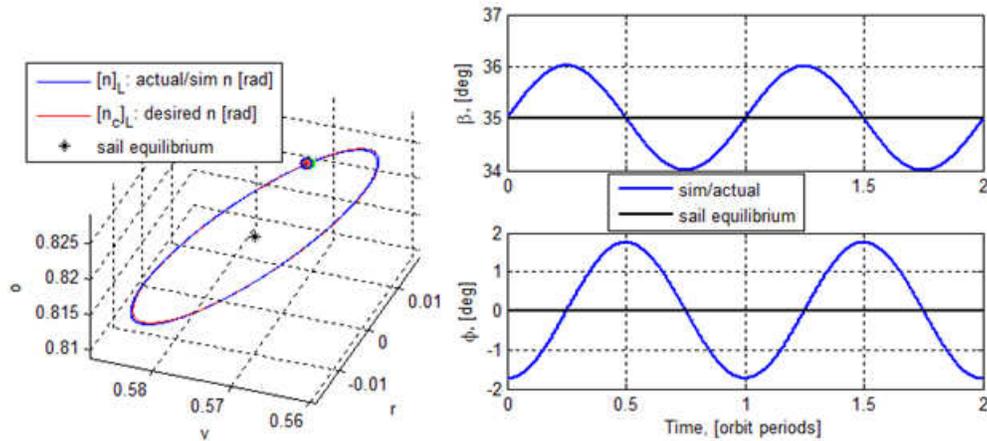
Figure 40: Sail Angular Positions for Coning Trajectory having Half Cone Angle, δ=1° about a Nominal Sail Normal of $\beta_0=35°$, $\Phi_0=0°$ in the L-frame, Equilibrium Spin

The simulation sail normal, $\hat{n}$ traces the desired circular cone. In addition, the cone and clock angles repeatedly complete one cycle in one orbital period. This indicates orbit rate coning. As compared with the zero sail spin (Figure 22), the coning tracing appears more accurate. To gain more confidence in this, the errors in the individual components of sail normal while tracing the desired cone are shown in Figure 41.
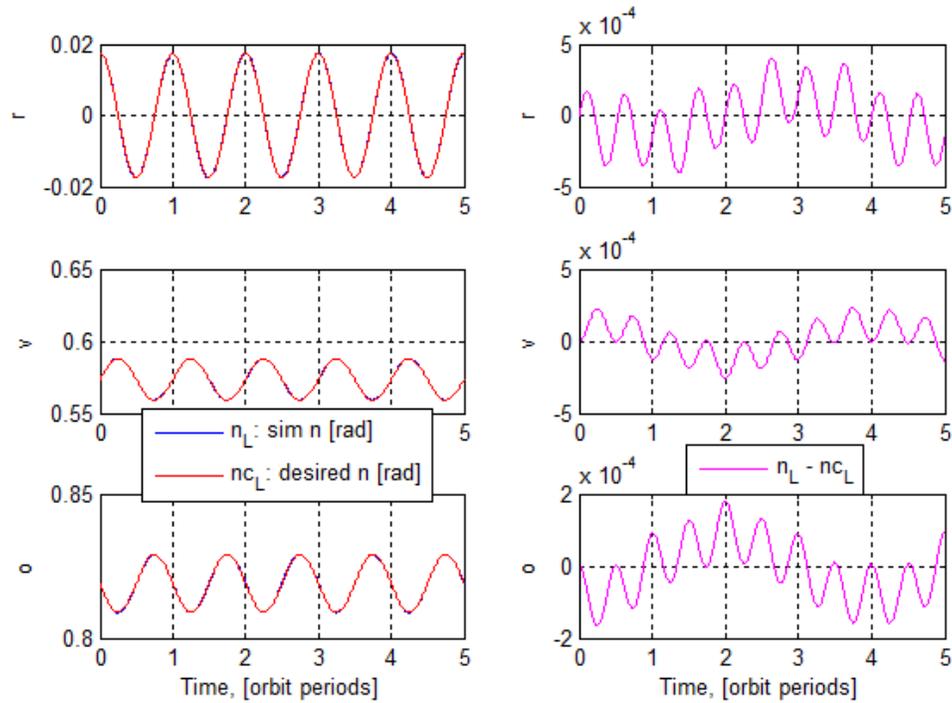
Figure 41: Individual L-frame Components of Simulated and Desired Sail Normal with Errors, Equilibrium Spin

As the cone is traced, the oscillating nature of the error magnitudes is similar to the ones in the zero sail spin. However, the magnitudes are 10 times lower in the equilibrium spin case (Figure 41) than the zero spin case (Figure 23). This means that the control method was able to provide better sail normal tracking at a lower cost (lower control torque magnitude) with the equilibrium spin as compared with the zero spin for this L-frame sail equilibrium point ($\beta = 35°, \phi = 0°$).

The performance of the control method with initial condition errors is analyzed and compared with the zero sail spin case below.
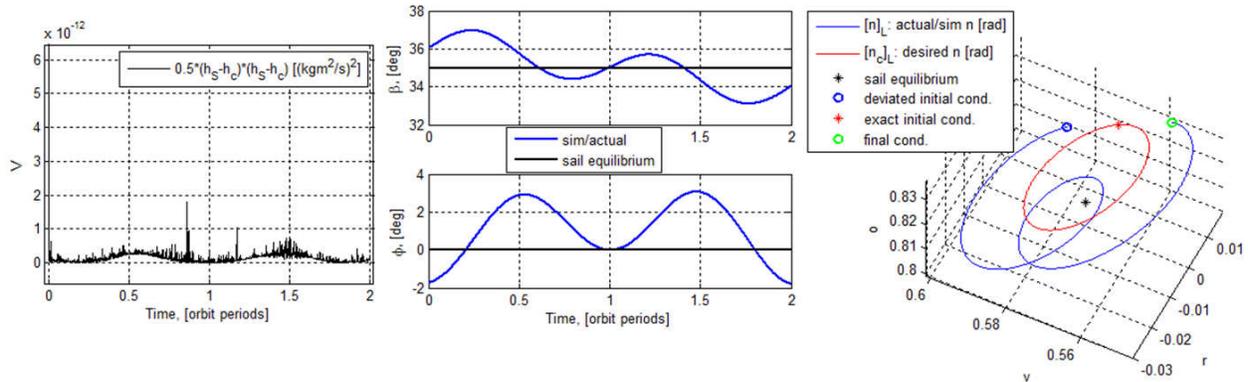
Figure 42: Control Method Performance in Tracking Desired Angular Momentum and Sail Normal with Initial Condition Error of 1° (d=1°), Equilibrium Spin

The Lyapunov function is on the same order of magnitude as for the zero sail spin case, indicating that the control method performance in reducing the angular momentum error is similar. However, the sail normal coning at orbit rate is better defined in the zero sail spin case. The cone and clock angles complete one revolution in one orbital period more closely than in the equilibrium spin case. The sail normal motion is also more circular in the zero sail spin case.
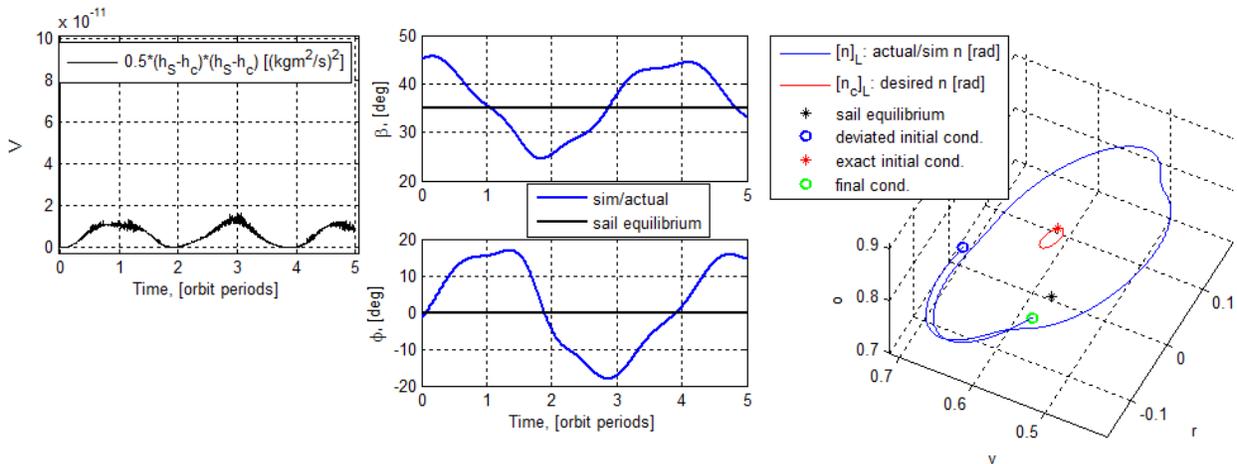
Figure 43: Control Method Performance in Tracking Desired Angular Momentum and Sail Normal with Initial Condition Error of 10° (d=10°), Equilibrium Spin

The Lyapunov function is on the same order of magnitude as in the zero sail spin case. However, the sail normal motion is neither at orbit rate nor does the sail normal trace the desired cone. The sail normal cones around the equilibrium point at a much slower rate (approx. once in 4 orbits) as compared with the zero sail spin case (approx. once every 1.25 orbits).

IV. CONCLUSION AND FUTURE WORK

Past work has shown that orbit rate coning of the sail normal vector about an LVLH attitude equilibrium point induces desired orbital effects and is unlikely to excite the structural sail dynamics. Sail attitude equilibria exist in the LVLH frame under the influence of gravity gradient, aerodynamic and solar torques. When the sail normal is precessed from some of these equilibria, the sail normal naturally cones about that equilibrium point. However, the sail normal coning has to follow a circular coning trajectory at orbit rate to induce the desired orbital effects. In this thesis, a control method is developed that enables sail normal coning (circular cones) about the LVLH attitude equilibria at orbit rate. The control method is designed such that the sail angular momentum tracks a desired trajectory.

The performance of the angular momentum error reduction control method was analyzed in this thesis. The control method caused the sail angular momentum to track the desired angular momentum on the coning trajectory over an orbit and reduced the initial angular momentum error in all cases studied. The method is robust to initial condition errors in tracking the desired angular momentum. Since angular momentum is a function of the sail angular position (sail normal), a reduction in angular momentum error was hoped to reduce the sail normal error between the sail normal and desired sail normal on the coning trajectory. This control method only functioned well for tracking the desired angular position (sail normal) at certain LVLH equilibrium points, for small cones and small initial condition errors. In the orbit lowering case ($\beta = 35°, \phi = 0°$), the control method allowed the sail normal to trace the desired sail normal on the circular coning trajectory at orbit rate. The coning was at orbit rate (accurate coning rate), but there were errors in the shape of the coning (inaccurate circular coning). Even though there were errors in the circular cone tracing (10 to 10^3 times lower than the absolute sail attitude), they

were bounded. In addition, past work asserted that the shape of coning need not be as accurate as long as orbit rate coning is achieved in order to attain the desired orbital effects. Thus, slight deviations from circular coning that cause these error magnitudes in the coning tracing are within the acceptable range. The performance of the control method deteriorated (deviated from orbit rate coning and had increased circular cone tracing errors) when the initial condition deviation was increased to 10° and cones became as large as 60°. Moreover, in the orbit raising case ($\beta = 145°, \phi = 180°$), the control method could not enable circular cone tracking at orbit rate. Therefore, the control method performed well in tracking the desired sail normal at certain equilibrium points, for smaller initial condition errors and for smaller cones. In these cases, the sail normal error remained small. The reason why the control method performed well with sail angular momentum and not the sail normal was because the sail normal errors cancelled with sail velocity errors in the angular momentum error term to yield a small angular momentum error even with large sail attitude and velocity errors.

For the cases where the desired sail normal tracking could occur at orbit rate, studies were performed on a spinning (spun at the equilibrium spin) and non-spinning sailcraft (zero sail spin) in order to determine the required control torque for inducing the desired coning. The required control torque is a combination of two control torque components: rate control torque and coning control torque. The rate control torque defines that piece of the total control torque which enforces orbit rate coning and allows the sail normal to trace the trajectory at the desired rate. The coning control torque is that piece which is used to induce the desired coning and allows the sail normal to trace the desired shape of the coning trajectory. It was argued that rate control torque is lower in the zero sail spin case (total angular momentum is lower for a non-spinning sail and thus the momentum vector is easier to precess), whereas the coning control

torque is lower for the equilibrium sail spin case (equilibrium sail spin causes natural coning that reduces the required control authority). It was interesting to determine which sail spin rate could result in the desired orbit rate circular coning with a lower cost (lower control torque magnitude). Even though, the required control torque was on the order of 10^{-6} Nm for both a spinning and non-spinning sail (10^{-6} Nm was found to be a reasonable torque magnitude from other work on small sailcraft with similar dimensions and mass properties), the required control torque was lower in magnitude with the equilibrium spin. For the equilibrium point used (orbit lowering case: $\beta = 35°, \phi = 0°$), the equilibrium spin case required ~4 times less control torque for the sail normal to stay on the desired circular coning trajectory at orbit rate. In addition, the equilibrium spin case provided a more effective control method performance in tracking the desired angular momentum and sail normal as compared with the zero sail spin case. In this case (specific equilibrium point) and with this result, the sail can be operated at the equilibrium spin rate. However when initial condition errors were added to the system, the zero sail spin case showed more robustness (better performance) in tracking the desired circular coning trajectory at orbit rate than the equilibrium sail spin case.

An extension of this thesis can take many interesting directions. Past work analyzed orbit rate coning for circular coning trajectories in order to induce the desired orbital effects. The assumption for circular coning can be relaxed and induced orbital effects for non-circular cones can be studied. A non-circular cone alters the sail normal thrust vector direction relative to the sun differently. This produces different orbital changes whose usefulness can be analyzed. This could relieve the control method from the need to provide perfectly circular cone tracing and only concentrate on enabling orbit rate coning. To better understand this control method, future work can include an understanding of why the desired sail angular momentum tracking does not

enable sail normal tracking at the same level of accuracy. It would be useful to see what drives the individual sail normal and velocity dependent terms in the angular momentum error equation to cancel each other, and to see this behavior can be prevented.

The results at the equilibrium point $\beta = 35°, \phi = 0°$ for the equilibrium sail spin revealed better performance in tracking the desired circular coning trajectory as compared to the zero sail spin case (10 times better) at a lower control torque cost (with no initial condition errors). The control torque calculation did not include the additional control torque that is required to operate the sail at the desired equilibrium sail spin (spin rate control torque). Further studies can include the magnitude of this spin rate control torque to make more accurate comparison with the control torque required in the zero sail spin case. In order to operate the sail at the equilibrium spin as opposed to having zero sail spin, the implications of providing extra mechanisms needed to spin the sail can also be explored. In addition, the relative control method performance from using the equilibrium and zero sail spins could be tested at other equilibrium points to see if the comparison between the two spin rates and conclusion drawn for this specific case hold in general.

The results here also indicate that the desired sail normal is traced more accurately (orbit lowering case) at some equilibria than at others (orbit raising case). In order to gain a better understanding of this phenomenon, linearized sail dynamics about the sail equilibria could be developed. Studying the near-equilibrium behavior may reveal why the desired sail normal is traced more accurately (orbit lowering case) at certain equilibrium points than at others (orbit raising case).

In this thesis, a flat, rigid sail model was used. A large, gossamer sail will not be perfectly flat or rigid in space. The dynamics can be more accurately captured by analyzing a realistic sail

shape. This work can be further extended to include non-flat, non-rigid sail dynamics. Finally, the practical implementation of the control torque required to enable the orbit rate coning of the desired trajectory with the existing hardware can be studied (e.g. using reaction wheels, tip vanes, or sailcraft bus deflection).

V. REFERENCES

[1] Botter, T., Coverstone, V. and Burton, R., "Structural Dynamics of Spin-Stabilized Solar Sails with Applications to UltraSail," *Journal of Guidance, Control and Dynamics*, Vol. 31, No. 2, 2008, pp. 402-413.

[2] Curtis, H., *Orbital Mechanics for Engineering Students*. Great Britain: Biddles Ltd, 2005.

[3] Derbes, B. and Lichodziejewski, D., "Residual Surface, Shape, and Mass Property Errors: Effects on Solar Sail Navigation and Attitude Control," *Proc. of AIAA/ASME/ASCE/AHS/ASC Structures, Structural Dynamics, and Materials Conf.*, AIAA 07-2414.

[4] Johnson, L., Young, R. and Montgomery, E., "Recent Advances in Solar Sail Propulsion System at NASA," *Acta Astronautica*, Vol. 61, No. 1-6, pp. 376-382.

[5] Lappas, V., Wie, B., McInnes, C., Tarabini, L., Gomes, L. and Wallace, K., "Microsolar Sails for Earth Magnetotail Monitoring," *Journal of Spacecraft and Rockets*, Vol. 44, No. 4, 2007, pp. 840-848.

[6] Lappas, V., Wokes, S., Leipold, M., Lyngvi, A. and Falkner, P., "Guidance and Control for an Interstellar Heliopause Probe (IHP) Solar Sail Mission to 200 AU," *Proc. of AIAA Guidance, Navigation and Control Conf.* AIAA 05-6085.

[7] Lawrence, D. and Piggott, S., "Integrated Trajectory and Attitude Control for a Four-Vane Solar Sail," *Proc. of AIAA Guidance, Navigation and Control Conf.* AIAA 05-6082.

[8] Lawrence, D. and Whorton, M., "Coning Control of Solar Sails Using Magnetic Momentum Error Reduction*," Journal of Spacecraft and Rockets*, Vol. 46, No. 6, 2009, pp. 1298-1308.

[9] Lawrence, D. and Whorton, M., "Solar Sail Dynamics and Coning Control in Circular Orbits," *Journal of Guidance, Control, and Dynamics*, Vol. 32, No. 3, 2009, pp. 974-985.

[10] Macdonald, M. and McInnes, C., "Analytical Control Laws for Planet-Centered Solar Sailing," *Journal of Guidance, Control and Dynamics*, Vol. 28, No. 5, 2005, pp. 1038-1048.

[11] Macdonald, M., Hughes, G., McInnes, C., Lyngvi, A., Falkner, P. and Atzei, A., "GeoSail: An Elegant Solar Sail Demonstration Mission," *Journal of Spacecraft and Rockets*, Vol. 44, No. 4, 2007, pp. 784-795.

[12] McInnes, C., Macdonald, M., Angelopolous, V. and Alexander, D., "GeoSail: Exploring the Geomagnetic Tail Using a Small Solar Sail," *Journal of Spacecraft and Rockets*, Vol. 38, No. 4, 2001, pp. 622-629.

[13] McMahon, J. and Lawrence, D. "Orbital Maneuvering with a Solar Sail Through the use of Natural Attitude Coning," *Proc. of AAS Astrodynamics Specialist Conf.* AAS 09-345.

[14] Mengali, G. and Quarta, A., "Near-Optimal Solar-Sail Orbit-Raising from Low Earth Orbit," *Journal of Spacecraft and Rockets*, Vol. 42, No. 5, 2005, pp. 954-958.

[15] Metter, E., Acikmese, B. and Ploen, S., "Attitude Dynamics and Control of Solar Sails with Articulated Vanes," *Proc. of AIAA Guidance, Navigation and Control Conf.*, AIAA 05-6081.

[16] Mettler, E. and Ploen, S., "Solar Sail Dynamics and Control Using a Boom Mounted Bus Articulated by a Bi-State Two-Axis Gimbal and Reaction Wheels," *Proc. of AIAA/AAS Astrodynamics Specialist Conf.*, AIAA 02-4992.

[17] Modi, V. and Shrivastava, S., "Satellite Attitude Dynamics and Control in Presence of Environmental Torques – A Survey," *Proc. of AIAA/AAS Astrodynamics Conf.*, AIAA 82-1414.

[18] Oyama, T., Yamakawa, H. and Omura, Y., "Orbital Dynamics of Solar Sails for Geomagnetic Tail Exploration," *Journal of Spacecraft and Rockets*, Vol. 45, No. 2, 2008, pp. 316-323.

[19] Papa, A. and Pellegrino, S., "Systematically Creased Thin-Film Membrane Structures," *Journal of Spacecraft and Rockets*, Vol. 45, No. 1, 2008, pp.10-18.

[20] Prado, J., Perret, A. and Dandouras, I., "Using a Solar Sail for a Plasma Storm Early Warning System," *ESA Symposium Proc. on Environment Modeling for Space-based Applications*, ESTEC, NL, 1996.

[21] Rizvi, F. and Lawrence, D. "Attitude Actuation Alternatives for Small Solar Sails," *Proc. of AAS Guidance and Control Conf.* AAS 09-083.

[22] Robertson, R., "Two Decades of Spacecraft Attitude Control," *Proc. of 18th AIAA Aerospace Sciences Meeting*, Huntsville, AL, Jan, 1978, AIAA 1978-7.

[23] Rotunno, M., Basso, M., Pome, A. and Sallusti, M., "A Comparison of Robust Attitude Control Techniques for a Solar Sail Spacecraft," *Proc. of AIAA Guidance, Navigation and Control Conf.*, AIAA 05-6083.

[24] Sakamoto, H., Miyazaki, Y. and Park, K., "Finite Element Modeling of Sail Deformation under Solar Radiation Pressure," *Journal of Spacecraft and Rockets*, Vol. 44, No. 3, 2007, pp. 514-521.

[25] Sands, N., "Escape from Planetary Gravity Fields by Use of Solar Sails," *ARS Journal*, Vol. 31, 1961, pp. 527-531.

[26] Schaub, H. and Junkins, J., *Analytical Mechanics of Space Systems (2nd Edition).* Virginia: AIAA, Inc., 2009.

[27] Stough, R., Heaton, A. and Whorton, M., "Chasing a Comet with a Solar Sail," Proc. *of AAS/AIAA Space Flight Mechanics Conf.*, AAS 08-171.

[28] Swartwout, M., "Earth Escape Using a Slowly Rotating, Doubly Reflective Sail," *Journal of Guidance, Control and Dynamics*, Vol. 28, No. 2, 2005, pp. 374-377.

[29] Thomas, S., Paluszek, M., Wie, B. and Murphy, D., "Design and Simulation of Sailcraft Attitude Control Systems Using the Solar Sail Control Toolbox," *Proc. of AIAA Guidance, Navigation and Control Conf.*, AIAA 04-4890.

[30] Wie, B., "Dynamic Modeling and Attitude Control of Solar Sail Spacecraft: Part I," *Proc. of AIAA Guidance, Navigation and Control Conf.*, AIAA 02-4572.

[31] Wie, B., "Dynamic Modeling and Attitude Control of Solar Sail Spacecraft: Part II," *Proc. of AIAA Guidance, Navigation and Control Conf.* AIAA 02-4573.

[32] Wie, B., Murphy, D., Paluszek, M. and Thomas, S., "Robust Attitude Control Systems Design for Solar Sails, Part I: Propellantless Primary ACS," *Proc. of AIAA Guidance, Navigation and Control Conf.*, AIAA 04-5010.

[33] Yamakawa, H., Funaki, I., Nakayama, Y., Fujita, K., Ogawa, H., Nonaka, S., Kuninaka, H., Sawai, S., Nishida, H., Asahi, R., Otsu, H. and Nakashima, H., "Magneto-plasma sail: An Engineering Satellite Concept and its Application for Outer Planet Missions," *Acta Astronautica*, Vol. 59, 2006, pp. 777-784.

VI. APPENDIX A

McMahon, J. et. al. have shown that for 1° cones, the greatest orbital effects occur at

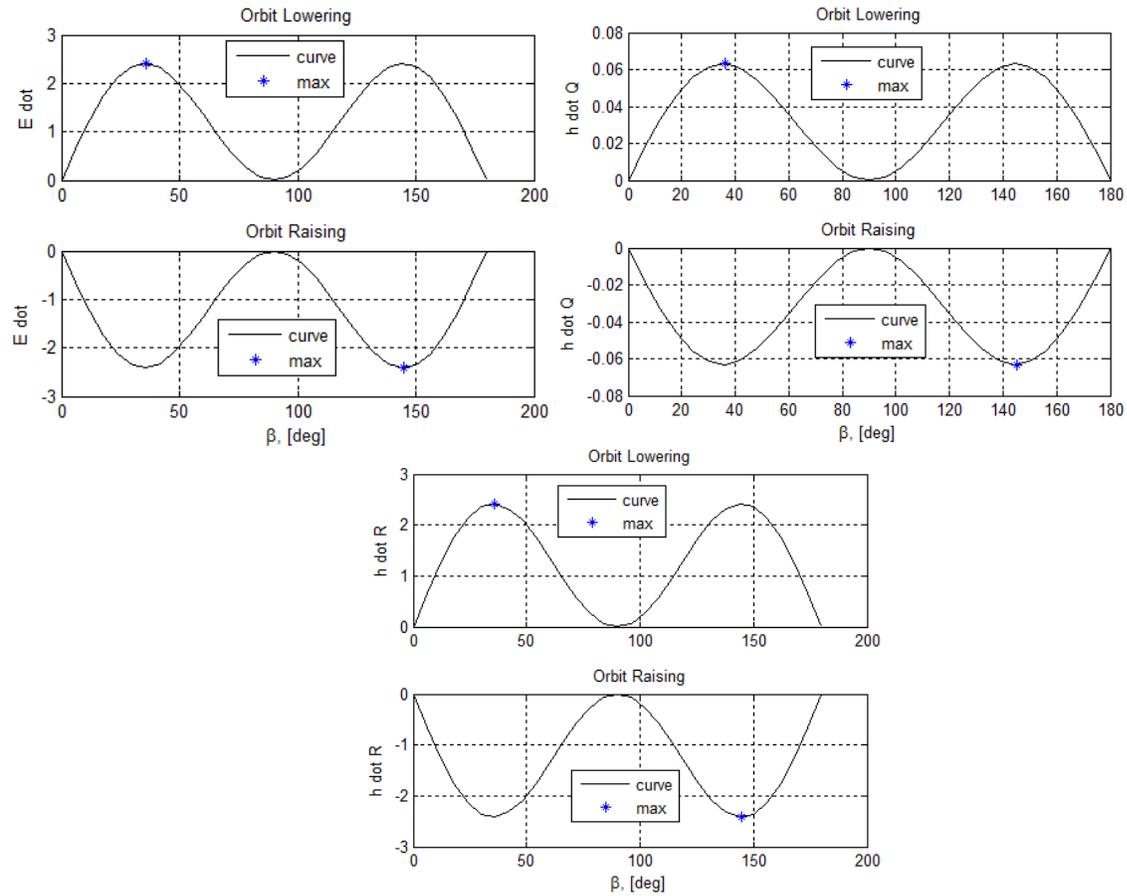$\beta = 35°, \phi = 0°$ for orbit lowering and $\beta = 145°, \phi = 180°$ for orbit raising [13].

Figure 44: Orbital Effects for Orbit Lowering (clock angle = 0°) and Raising (clock angle = 180°) over Cone Angle